nature structural & molecular biology

Structural and functional bases for broad-spectrum neutralization of avian and human influenza A viruses

Jianhua Sui[1,4], William C Hwang[2,4], Sandra Perez[3], Ge Wei[2], Daniel Aird[1], Li-mei Chen[3], Eugenio Santelli[2], Boguslaw Stec[2], Greg Cadwell[2], Maryam Ali[1], Hongquan Wan[3], Akikazu Murakami[1], Anuradha Yammanuru[1], Thomas Han[1], Nancy J Cox[3], Laurie A Bankston[2], Ruben O Donis[3], Robert C Liddington[2] & Wayne A Marasco[1]

Influenza virus remains a serious health threat, owing to its ability to evade immune surveillance through rapid genetic drift and reassortment. Here we used a human non-immune antibody phage-display library and the H5 hemagglutinin ectodomain to select ten neutralizing antibodies (nAbs) that were effective against all group 1 influenza viruses tested, including H5N1 'bird flu' and the H1N1 'Spanish flu'. The crystal structure of one such nAb bound to H5 shows that it blocks infection by inserting its heavy chain into a conserved pocket in the stem region, thus preventing membrane fusion. Nine of the nAbs employ the germline gene *VH1-69*, and all seem to use the same neutralizing mechanism. Our data further suggest that this region is recalcitrant to neutralization escape and that nAb-based immunotherapy is a promising strategy for broad-spectrum protection against seasonal and pandemic influenza viruses.

Seasonal influenza A is a scourge of the young and old, killing more than 250,000 worldwide each year, while creating an economic burden for millions[1]. Pandemic influenza, which occurs when a new virus emerges and infects people globally that have little or no immunity, represents a grave threat to human health; for example, the 1918 Spanish Flu pandemic caused an estimated 50 million deaths[2,3]. Vaccines have historically been the mainstay of infection control. However, owing to rapid antigenic drift, the vaccine antigen must be updated annually based on global influenza surveillance[4,5], and it is not always fully successful. In addition, some recent H5N1 vaccines have shown promising results[6–9], but none has been reported to elicit a broad neutralizing response in humans. Neuraminidase inhibitors, especially oseltamavir (Tamiflu), remain the primary treatment, but they have limited efficacy if administered late in infection, and widespread use is likely to result in the emergence of resistant viral strains[10,11].

Influenza A is subclassified by its two major surface proteins: hemagglutinin, which mediates cell entry, first by recognizing host proteins bearing sialic acid on their surface, and second by triggering the fusion of viral and host membranes following endocytosis, allowing viral RNA to enter the cytoplasm; and neuraminidase, which cleaves sialic acid from host and viral proteins, facilitating cell exit[12]. There are 16 hemagglutinin subtypes (H1–16) and 9 neuraminidase subtypes (N1–9) that make up all known strains of influenza A viruses by various combinations of hemagglutinin and neuraminidase[12] (**Supplementary Fig. 1** online).

The recent spread of highly pathogenic avian influenza (HPAI), caused by the H5N1 strain, across Asia, Europe and Africa raises the specter of a new pandemic, should the virus mutate to become readily transmissible from person to person. The evolution of H5N1 into a pandemic threat could occur through a single reassortment of its segmented genome or through the slower process of genetic drift[12,13]. Nearly 400 human H5N1 infections have been reported since 1997 from 14 countries, with a case mortality rate in the immunocompetent population above 60%[4].

New therapeutic strategies that provide potent and broadly cross-protective host immunity are therefore a global public health priority. Human mAb-based 'passive' immunotherapy is now being used to treat numerous human diseases, including respiratory syncytial virus infection, and we have proposed how immunotherapy could be used strategically in a viral outbreak setting[14].

In the present study, we first used a phage-display antibody library and recombinant H5 trimeric ectodomain to isolate a group of high-affinity nAbs that were potent inhibitors of H5N1 viral infection *in vitro* and *in vivo*. On the basis of crystallographic and functional studies, we showed that the nAbs bind to a common epitope—a highly conserved pocket in the stem region of hemagglutinin containing the 'fusion peptide'—that rationalizes their ability to block

[1]Department of Cancer Immunology & AIDS, Dana-Farber Cancer Institute; Department of Medicine, Harvard Medical School, 44 Binney Street JFB 826, Boston, Massachusetts 02115, USA. [2]Infectious and Inflammatory Disease Center, Burnham Institute for Medical Research, 10901 North Torrey Pines Road, La Jolla, California 92037, USA. [3]Influenza Division, Centers for Disease Control and Prevention, National Center for Immunization and Respiratory Diseases, 1600 Clifton Road, Mail Stop G-16, Atlanta, Georgia 30333, USA. [4]These authors contributed equally to this work. Correspondence should be addressed to J.S. (jianhua_sui@dfci.harvard.edu), R.O.D. (rvd6@cdc.gov), R.C.L. (rlidding@burnham.org) or W.A.M. (wayne_marasco@dfci.harvard.edu).

Received 18 November 2008; accepted 22 January 2009; published online 22 February 2009; doi:10.1038/nsmb.1566

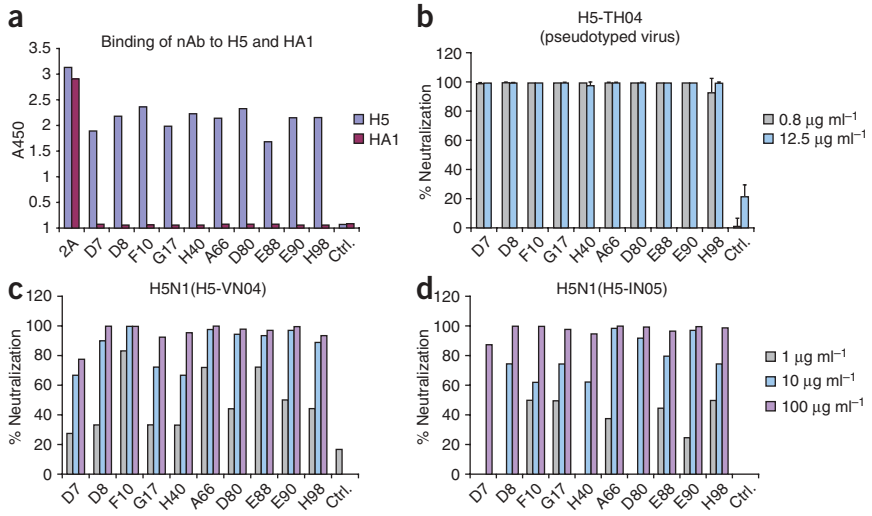

Figure 1 *In vitro* binding and neutralization of anti-H5 antibodies. (**a**) The ten antibodies were converted to soluble scFv-Fcs (scFv linked to the hinge, CH2 and CH3 domains of human IgG1) and evaluated for binding to trimeric H5-TH04 or monomeric HA1 of H5-TH04 coated on an ELISA plate. The H5 scFv-Fcs recognize trimeric H5 but not HA1. An antibody raised against HA1 (2A) recognized both. (**b**) Neutralization of H5-TH04–pseudotyped viruses (virus-like particles with HIV-1 only cores that display H5 on their surface). Percentage of neutralization at two concentrations is shown with s.d. The mAb 80R[18] was used as a negative control (Ctrl.). (**c**,**d**) Neutralization of wild-type H5-VN04 and H5-IN05 by the ten scFv-Fcs at three concentrations using a plaque reduction assay. Results are consistent with those obtained from a microneutralization assay (data not shown).

membrane fusion rather than cell attachment. Sequence and structural analysis of all 16 hemagglutinin subtypes point to the existence of just two variants of this epitope, corresponding to the two classic phylogenetic groupings of hemagglutinin (groups 1 and 2). We therefore tested eight more group 1 hemagglutinin subtypes and demonstrated an unprecedented cross-subtype binding and/or neutralization spectrum. Because we had used a group 1 subtype (H5) for our panning, our nAbs, as expected, failed to neutralize group 2 subtypes H3 and H7. These results nevertheless raise the possibility that a cocktail comprising a small subset of nAbs raised against representatives of the two groups could provide broad protection against all seasonal and pandemic influenza A viruses.

RESULTS

Identification of nAbs against H5N1

The current H5N1 epidemics involve viruses derived from a single lineage of H5 hemagglutinin. Within this lineage, four distinct clades have been identified as major threats to public health[15,16]. We expressed recombinant trimeric ectodomain of H5 hemagglutinin from one of these viruses (strain A/Vietnam/1203/04 (H5N1), 'H5-VN04', clade 1) in insect cells[17] (**Supplementary Fig. 2** online), immobilized it on a plastic surface and selected antibodies from a 'non-immune' human antibody phage-display library (using single-chain VH-VL fragments ('scFv'))[18]. Two rounds of panning and the screening of 392 clones identified 10 unique antibodies formed by six distinct VH (variable region of heavy chain) fragments in combination with ten different VL (variable region of light chain) fragments (**Supplementary Table 1** online).

We found that all ten nAbs bound trimeric H5-VN04 with similar avidity, but did not bind monomeric HA1 (**Fig. 1a**). Presented as scFv-Fc constructs, they potently neutralized the clade 1 H5 pseudovirus, A/Thailand/2-SP-33/2004 (H5N1) ('H5-TH04') (**Fig. 1b**); and, in a stringent plaque-reduction assay, they all showed high levels of neutralization against H5-VN04, as well as the more divergent (clade 2.1) A/Indonesia/5/2005 ('H5-IN05') (**Fig. 1c**,**d**). We further found that the nAbs cross-competed with each other in a competition enzyme-linked immunosorbent assay (ELISA; **Supplementary Fig. 3** online), suggesting that they share a common epitope. On the basis of this finding, as well as VH sequence diversity and neutralization potency, we converted three of the nAbs (D8, F10 and A66) into full-length human IgG1s for further studies; all three IgG1s bound to recombinant H5-VN04 with high affinity (K_d ~100–200 pM) and slow dissociation rates (k_d ~10^{-4} s^{-1}) (**Supplementary Fig. 4** online).

Prophylactic and therapeutic efficacy in mice

We evaluated the protective efficacy of the three IgG1s against H5N1 virus infection in a BALB/c mouse model (**Fig. 2**). Mice were treated with IgG1s before (prophylactically) or after (therapeutically) lethal viral challenge. Prophylaxis using 10 mg kg^{-1} of IgG1s effectively protected (80–100%) mice when challenged with a high lethal dose of H5-VN04 (clade 1) or A/HongKong/483/97 ('H5-HK97') (clade 0) (**Fig. 2a**,**b**). Therapeutic treatment with 15 mg kg^{-1} (an achievable dose in humans) of IgG1 24 h post-inoculation (hpi) also protected 80–100% of the mice challenged with either H5-VN04 or H5-HK97 virus (**Fig. 2c**,**d**). Mice treated at later times (48 hpi or 72 hpi) with H5-VN04 showed similar or higher levels of protection (**Fig. 2e**,**f**). Furthermore, surviving mice remained healthy and showed minimal body weight loss over the 2-week observation period (data not shown).

Whereas human influenza viruses are typically restricted to the upper respiratory tract, systemic spread is a typical outcome of H5N1 infection in mice, and it has been reported in some humans. We found that the three IgG1s caused potent suppression of viral replication in the lungs (measured 4 d after viral challenge) of mice treated within 48 h of viral challenge; and that two IgG1s, F10 and A66, were effective when given at 72 hpi. The strong impact of antibody therapy on systemic infection was demonstrated by ≥1,000-fold suppression of virus spread to the spleen, even when given 72 hpi (**Supplementary Fig. 5** online). We also observed suppression in the brain, but in this case, systemic spread was too low in control animals for accurate quantitation.

nAbs inhibit cell fusion rather than receptor binding

Two ways in which anti-hemagglutinin antibodies can neutralize infection is by blocking the initial binding of hemagglutinin to its cellular receptor (sialic acid) or by interfering with the subsequent step of hemagglutinin-mediated virus-host membrane fusion, which occurs in acidic endosomes[19,20]. We found that none of the nAbs inhibited virus binding to cells (**Fig. 3a**) or hemagglutination of red blood cells (data not shown). However, we were able to show, using a model system of cell fusion, that the nAbs potently inhibited membrane fusion (**Fig. 3b**).

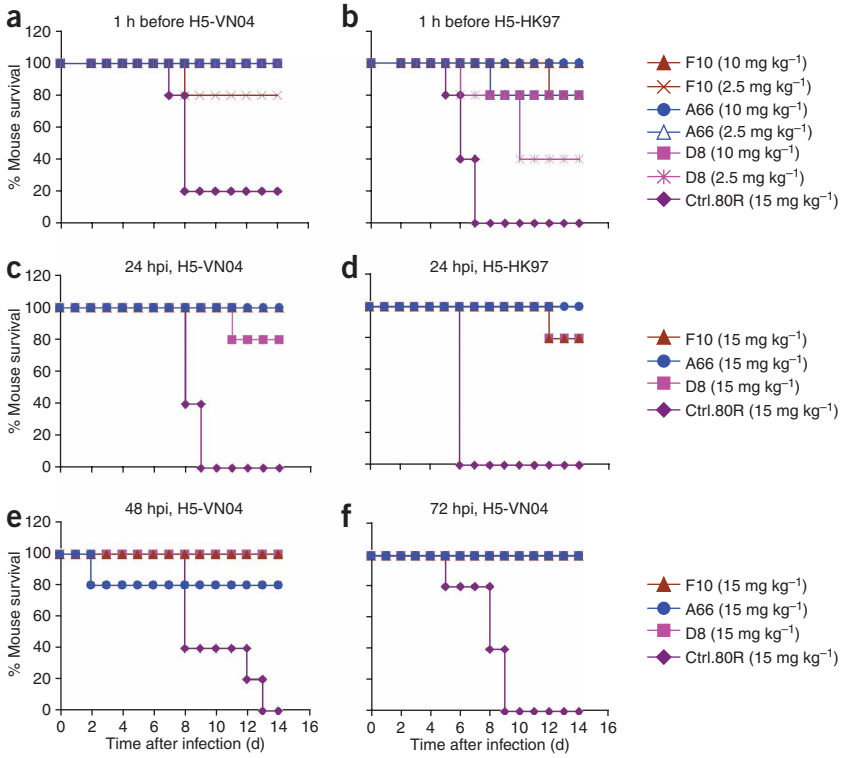

Figure 2 Prophylactic and therapeutic efficacy of anti-H5 nAbs in mice. (**a**,**b**) Prophylactic efficacy. Percentage of survival of mice treated with anti-H5 nAbs or control mAb 1 h before lethal challenge by intranasal inoculation with H5-VN04 (**a**) or H5-HK97 (**b**) viruses. (**c**–**f**). Therapeutic efficacy. Mice were inoculated with H5-VN04 and injected with nAbs at 24 h, 48 h of 72 hpi (**c**,**e**,**f**) or with H5-HK97 at 24 hpi (**d**).

Structural characterization of the nAb epitope

To provide a structural basis for neutralization and to explore the prospects for developing even broader-spectrum therapeutics, we determined the crystal structure of F10 (as the scFv fragment) in complex with the H5 (H5-VN04) ectodomain (**Fig. 4** and **Supplementary Table 2** online). We used H5 activated by cleavage of the single-chain precursor, HA0, into two polypeptides, HA1 and HA2. Cleavage leads to the partial burial of the fusion peptide (the first ~21 residues of each HA2) into the stem[19,21], which also contributes to the formation of each of three hydrophobic 'pockets' located below the large trimeric receptor binding head. In the complex, one F10 nAb binds into each pocket, burying ~1,500 Å^2 of protein surface. Only the heavy chain (VH) participates directly in binding, using all three of its complementarity-determining regions (CDRs). The light chain (VL) points out into solution and makes only nonspecific contacts with the distal end of the oligosaccharide of glycosylated residue $Asn33_1$ from a neighboring monomer. The epitope on H5 encompasses the entire pocket, which is formed by the HA2 fusion peptide flanked by elements of HA1 on one side and helix αA of HA2 on the other.

The key interactions are as follows (**Fig. 4b**). (i) CDR-H2 adopts the 'type 2' conformation[22]. Two hydrophobic residues, Met54 and Phe55, from the tip of H2 insert into the pocket. Phe55 lies across a flat hydrophobic surface formed by the main chain of the fusion peptide, residues 18_2–21_2; it also makes favorable orthogonal aromatic interactions[23] with the side chains of $Trp21_2$ at the back of the pocket and $His18_1$ at the front (subscripts 1 or 2 refer to HA1 or HA2, and the numbering scheme follows the structure of H3 (PDB 2HMG)[17,24]). The Met54 sulfur makes Π−aromatic interactions[25] with the $Trp21_2$ ring, hydrophobic interactions with $Ile45_2$ from helix αA and a hydrogen bond between Met54 C=O and the $His38_1$ side chain. (ii) Tyr102 from CDR-H3 extends from the apex of the H3 loop to a location only ~3 Å from Phe55, and it complements CDR-H2 by cementing together the fusion peptide (via a main chain hydrogen bond to $Asp19_2$) and the αA helix of HA2 (by intercalating between $Thr41_2$ and $Ile45_2$). A large hydrophobic residue at the neighboring position 103 supports the side chain conformation of Tyr102. (iii) The CDR-H1 loop is characterized by small hydrophobic or polar side chains (notably Val27, Thr28 and Ser31) such that CDR-H1 fits snugly beneath the hemagglutinin head while packing against helix αA. A somatic mutation of conserved Gly26, G26E, generates a noncanonical conformation for H1, with Thr27 pointing outward and making contact H5.

An N-terminal hairpin (residues $Ile29_2$ and $Met30_2$) from HA2 of the counterclockwise neighbor packs against the other side of helix αA at this point, wrapping around its fusion peptide and further locking it into place (**Fig. 4a**,**c**). Thus, the F10 nAb may stabilize the fusion peptide of more than one subunit. One framework (FR3) residue, Gln74, seems to be especially important in stabilizing the CDR-H1 and CDR-H2 loop conformations, by forming hydrogen bonds to the main chain C = O groups of Pro53 and Met54, as well as the side chain of Ser30. The FR3 residue at position 72 is the major determinant of the choice between two distinct conformations of the H2 loop[22].

Consistent with the structural data, mutations in three H5 residues on HA2 αA, $Val52_2$, $Asn53_2$ and $Ile56_2$, which make important interactions with F10, greatly reduce or ablate nAb binding, whereas the conservative mutation V52L has no effect (**Fig. 4c**,**d**). Mutations to other surfaces of the αA helix either have no effect (typically exposed residues) or lead to increased nAb binding, perhaps by subtly increasing the flexibility of the epitope (**Fig. 4d**). Notably, the nine other nAbs show similar mutant binding profiles. Together with the cross-competition noted above, this strongly suggests that the epitopes for all ten nAbs overlap very closely indeed, and that the nAbs bind in a similar location and orientation.

Structural basis of H5 neutralization by the nAb panel

The broad neutralizing behavior against H5 may be attributed in part to the exclusive role of VH in antigen binding and the use of a common germline gene, *VH1-69*, in five out of the six VHs, although their CDR3 loops are variable in sequence and length (13–17 residues) (**Supplementary Fig. 6** and **Supplementary Table 1** online). In addition, free-energy calculations[26] point to dominant binding contributions (~70% of the total favorable free energy) of the three conserved residues in the VH segment (**Fig. 4b**). In CDR-H2 derived from germline *VH1-69*, position 55 is always phenylalanine, and position 54 is always hydrophobic (methionine, isoleucine, leucine or valine). In our nAbs, CDR-H3 always has a tyrosine predicted to lie at the tip of the CDR3 loop (conserved at the position 6). The

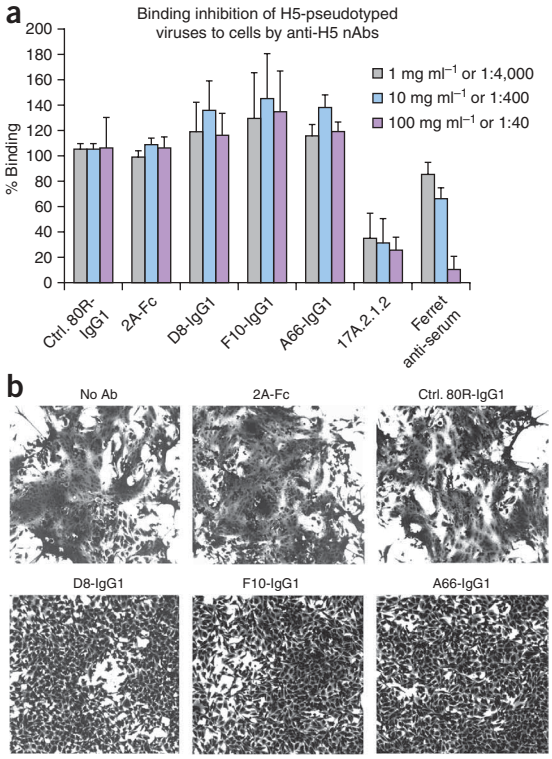

Figure 3 Neutralization mechanism. (**a**) nAbs do not inhibit cell binding of full-length hemagglutinin from H5-TH04–pseudotyped HIV-1 viruses. None of the three nAb-treated viruses inhibited cell binding. Mouse anti-H5 mAb, 17A2.1.2 and ferret anti-H5N1 serum, which inhibit hemagglutination, were used as positive controls. Anti-SARS spike protein (80R) and anti-HA1 (2A) were used as negative controls. Error bars represent s.d. (**b**) All three nAbs inhibit cell fusion. HeLa cells were transfected with H5-TH04–expressing plasmid and exposed to a pH 5.0 buffer for 4 min in the presence or absence of nAbs. Syncytia formation induced by the brief exposure to pH 5.0 was completely inhibited by D8, F10 and A66, at 20 μg ml^{-1} (~0.13 μM), whereas controls (80R and anti-HA1 mAb (2A) at the same concentration had no effect.

conformation and sequence of the CDR1 loop does not seem to be critical, because the other antibodies we isolated do not contain the somatic mutation (G26E) found in F10 and are predicted to have canonical structures. The sixth VH gene we isolated is derived from the germline gene *VH1-2*; its H2 loop has the same length as *VH1-69*, but by virtue of a change from alanine to arginine at position 72 (ref. 22) it is predicted to adopt a distinct conformation ('type 3') that presents loop residues 3 and 4 to the antigen (rather than residues 4 and 5 in type 2 loops). The specific somatic mutation at position 4, from asparagine to methionine, presumably promotes H5 binding. It is not possible to predict the structure of the larger H3 loop, but a tyrosine located at the center of the loop may play an analogous role to that in F10.

Thus, the F10-H5 crystal structure suggests a common mechanism of H5 virus neutralization for our nAb panel. They make no contact with the receptor binding sites in the head and so do not inhibit cell attachment. Rather, they lock the fusion peptide and helix αA in place, thereby preventing the large structural reorganizations that are required for membrane fusion[17,19,27–30]. Our data point to this event occurring at an early step in infection, although we cannot rule out the possibility that the nAbs act at a later stage, given the close packing of molecules on the surface of the mature virion, which might restrict early access to the epitope. The only previously published crystal structure of a hemagglutinin-nAb complex that inhibits membrane fusion uses a different mechanism: it prevents conformational changes by cross-linking the upper surfaces of adjacent subunits in the head[31].

NAbs bind and neutralize a broad range of group 1 viruses

Next we examined all of the available hemagglutinin sequences (total 6,360) in the public influenza sequence database (**Supplementary Table 3** online). Of note, the sequences of the F10 epitope are nearly always conserved within the H5 subtype. Indeed, many epitope residues, especially in HA2, are highly conserved across all 16 hemagglutinin subtypes (**Fig. 5**). This high sequence conservation

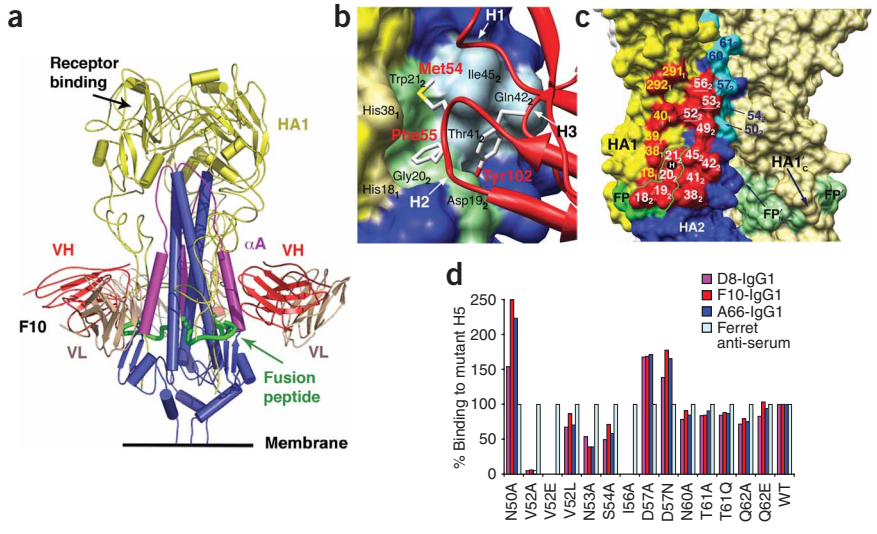

Figure 4 Structure of the H5–F10 complex. (**a**) Structure of the H5 trimer bound to F10 (scFv). H5 is similar to the uncomplexed structure[35] (pairwise r.m.s. deviation (Cα) = 1.0 and 0.63 Å for two independent trimers). HA1, HA2, the αA helix of HA2, the fusion peptide (FP) and F10 (VH and VL) are color coded. The third F10 molecule is hidden behind the stem. (**b**) Close-up of the epitope showing H5 as a molecular surface, with selected epitope residues labeled. The fusion peptide is in green. The tip of F10 (red ribbon) and selected CDR side chains are shown. Of 1,500 Å^2 buried surface at the interface, 43% involves hydrophobic interactions. (**c**) Surface of the central stem region, showing two H5 monomers. One monomer has HA1 (yellow) and HA2 (blue) colored differently; the path of the FP through the epitope (red) is outlined, and mutations that do not affect binding are colored cyan (**Fig. 4d**). The fusion peptides (FP and FP′) are labeled in both monomers. Epitope residues are labeled white (HA2) or yellow (HA1), and the position of buried residue H111$_2$ is shown as a black ball labeled 'H'. (**d**) Binding of the three nAbs to H5 mutants in the αA helix, transiently transfected into 293T cells. Note the similar response to all mutants tested. Mutations were made either to alanine or to the corresponding H7 residue; 24 h after transfection, nAbs or ferret anti-H5N1 serum was used to stain the transfected cells. Fluorescent intensity was normalized against ferret anti-serum (100%) to account for different expression levels.

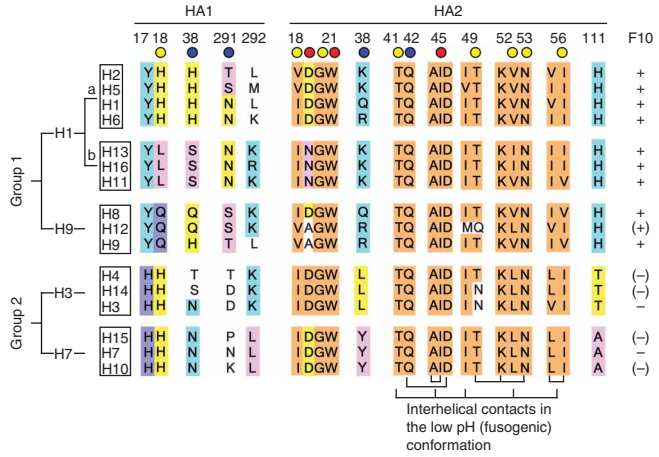

Figure 5 Sequence conservation in hemagglutinin groups, clusters and subtypes at the F10 epitope. Circles below residue numbers indicate estimated contribution to the binding energy at each position: red, strong; yellow, intermediate; blue, neutral. Residues without a circle are not directly involved in the epitope but are discussed in the text. Colored highlighting on the sequences indicates conservation within clusters and groups, with orange indicating high conservation or invariance. Other colors (for example, yellow, cyan and pink) highlight residues that are cluster or subtype specific. The network of interhelical contacts that stabilize the fusogenic structure[61] are indicated below the HA2 sequences. Subtypes that can be recognized/neutralized by F10 are indicated with '+' on the far right. (+) or (−) indicates a predicted positive or negative binding, respectively.

provides a rationale for the cross-neutralization of the H5N1 virus clades described above, and this prompted us to test our antibodies against a broader range of hemagglutinin subtypes.

Group 1 viruses, which contain 10 of the 16 subtypes, are further classified into three 'clusters': H1a, H1b and H9 (refs. 32,33; **Fig. 5**). We tested nAb binding to eight members of clusters H1a, H1b and H9, which include avian H5 and the most common human influenza subtypes (the major exception is the group 2 subtype, H3). In addition to H5, we found that all three IgG1s bound to cells expressing full-length H1 from three different strains of H1N1, including the 1918 Spanish flu, H2 from H2N2 and H6 from H6N2, the Cluster 1b subtypes H11 from H11N9, H13 from H13N6 and H16 from H16N3, and the Cluster H9 subtypes from three H9N2 strains. However, none of them bound to a group 2 subtype, H7 from H7N1 (**Supplementary Fig. 7** online).

The IgG1s also neutralized H5-, H1-, H2-, H6- and H11-pseudotyped virus infections (**Fig. 6a**). In a microneutralization assay, F10-IgG1 also neutralized H5N1, H1N1, H2N2, H6N1, H6N2, H8N4 and H9N2 influenza viruses (**Fig. 6b**). However, none of the nAbs neutralized group 2 viruses, for example, H3N2 (**Fig. 6b** and **Supplementary Fig. 8** online). Thus, these nAbs recognize an epitope on hemagglutinin that is conserved among H5 clades and in all members of group 1 viruses. Finally, we demonstrated the *in vivo* protective efficacy of two of the IgG1s against two lethal H1N1 viral strains in a BALB/c mouse model, using the same protocol as for the H5N1 studies (**Fig. 6c,d**).

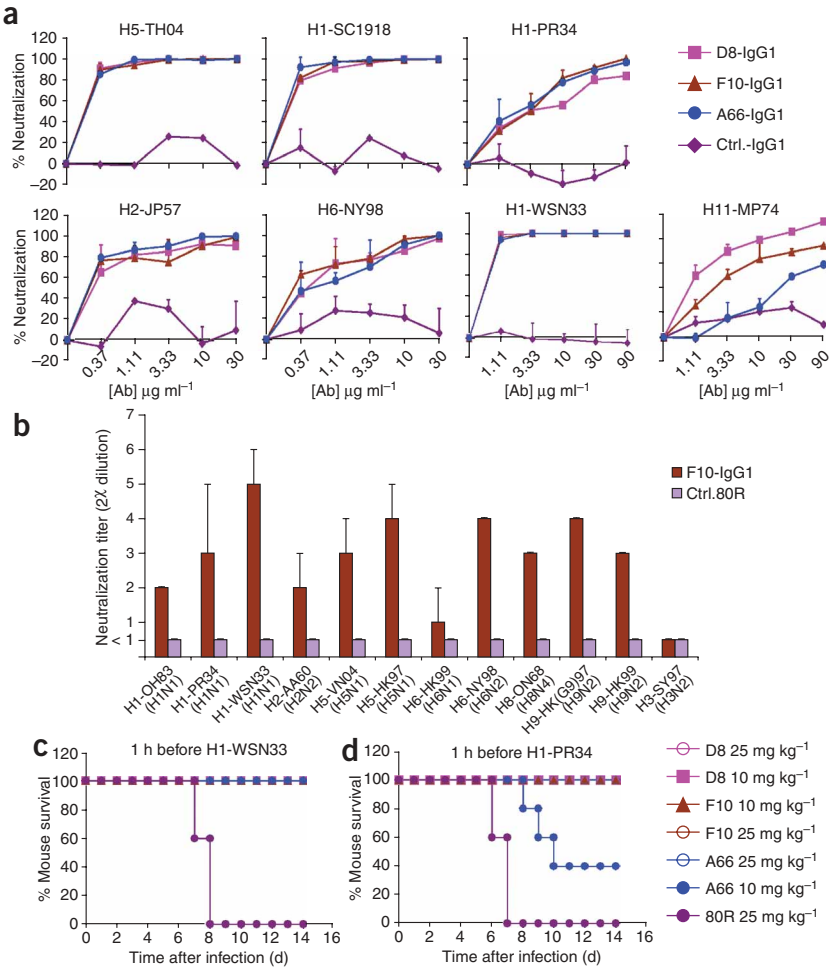

Figure 6 Cross-subtype neutralization by nAbs. (**a**) nAbs D8, F10 and A66 all neutralized indicated pseudotyped viruses (strains described below). Error bars indicate s.d. (**b**) Microneutralization assay. Neutralization titers (0.1 mg ml^{-1} antibody stock solution) of nAb F10 against wild-type H5N1, H1N1, H2N2, H6N1, H6N2, H8N4, H9N2 and H3N2 virus strains. 80R is the negative control. Vertical bars and whiskers represent the lowest and the highest neutralization titer (2^{χ}, values of χ are shown on the *y* axis), respectively, of two or three independent experiments. (**c**,**d**) Prophylactic efficacy against two H1N1 strains in mice. Percentage of survival of mice treated with anti-H5 nAbs or control mAb are shown before lethal challenge by intranasal inoculation with H1-WSN33 (**c**) or H1-PR34 (**d**) viruses. Complete viral strain designations are: H1-OH83 (A/Ohio/83 (H1N1)); H1-PR34 (A/Puerto Rico/8/34 (H1N1)); H1-SC1918 (A/South Carolina/1/1918 (H1N1)); H1-WSN33 (A/WSN/1933 (H1N1)); H2-AA60 (A/Ann Arbor/6/60 (H2N2)); H2-JP57 (A/Japan/305/57(H2N2)); H3-SY97 (A/Sydney/5/97(H3N2)); H6-HK99 (A/quail/Hong Kong/1721-30/99(H6N1)); H6-NY98 (A/chicken/New York/14677-13/1998 (H6N2)); H7-FP34 (A/FPV/Rostock/34 (H7N1)); H8-ON68 (A/turkey/Ontario/6118/68); H9-HK(G9)97 (A/chicken/HongKong/G9/97 (H9N2)); H9-HK99 (A/HongKong/1073/99 (H9N2)); H11-MP74 (A/duck/Memphis/546/74 (H11N9)).

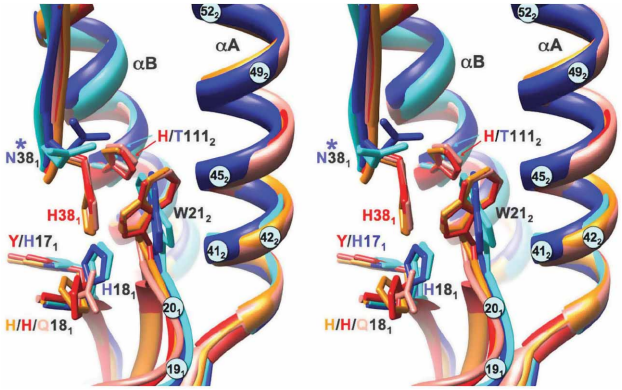

Figure 7 Three-dimensional comparison of the F10 epitope in group 1 and group 2 hemagglutinins. Stereo overlay of crystal structures of the five known hemagglutinin subtypes in the region of the F10 epitope, showing conservation and differences between the two phylogenetic groups. H1, H5 and H9 (group 1) are in shades of red and yellow (PDB 1RU7, 2IBX and 1JSD); H3 and H7 (group 2) are in shades of blue (PDB 1MQL and 1TI8). R.m.s. differences for pairwise overlays are 0.56 ± 0.11 Å (observed range, group 1), 0.75 Å (group 2) and 1.21 ± 0.12 Å between groups. Consistent differences between phylogenetic groups include the orientation of $Trp21_2$ and alternative side chain directions at 18_1 and 38_1, which are linked to the packing of buried $His111_2$ (the putative pH trigger in group 1; absent in group 2), and the burial of the larger tyrosine (group 1) versus histidine (the putative pH trigger in group 2) at 17_1. Of particular note, $Asn38_1$ is glycosylated in four members of the group 2 clusters. Other epitope residues are indicated by numbered light blue circles.

Basis of the group-specific broad-spectrum virus neutralization

The ability of our nAbs to recognize all group 1 (cluster H1a/b and H9) viruses (H12 was not tested) can be attributed to the key conserved features of the nAbs described above in combination with the highly conserved pocket on hemagglutinin (**Figs. 4** and **5**). The epitope may be divided into three elements. (i) At its center, the sequence of the N-terminal segment of HA2—fusion peptide residues 18_2–21_2—is conserved across all hemagglutinin subtypes (note that the side chain at position 19_2 does not participate in binding). (ii) A downstream segment of HA2 adopts part of the αA helix (residues 39_2–56_2), which is nearly invariant; the only significant difference is a threonine to glutamine change at position 49_2 in the untested H9 cluster subtype, H12. $Thr49_2$ lies at the periphery of the epitope and makes one long hydrogen bond (3.5 Å) to Ser31. Simple modeling suggests that there is plenty of space to accommodate the larger glutamine side chain and that it can make comparable hydrogen bonds. (iii) Smaller contributions from segments of the HA1 chain (residues 18_1 and 38_1) and a loop at the base of the head (residues 291_1 and 292_1).

Three-dimensional comparisons of the epitope in the five known crystal structure subtypes (three from group 1 (H1, H5 and H9) and two from group 2 (H3 and H7)[21,32,34–36]) show that they adopt two distinct structural classes consistent with the phylogenetic groupings[32,33] (**Fig. 7**). These differences arise from group-specific differences in the location of buried residues, notably histidines ($H111_2$ is unique to group 1; $H17_1$ is unique to group 2) that have been proposed to be the 'triggers' for pH-induced conformational changes[29]. The differences cause the side chain of $Trp21_2$ to turn through 90° in group 2 subtypes, eliminating favorable binding to Phe55 from our nAb panel. In addition, four out of six group 2 subtypes are glycosylated at position 38_1, at the periphery of the F10 epitope; our modeling studies predict steric clashes with the CDR-H1 loop (data not shown). These structural differences rationalize the observed lack of binding and neutralization of group 2 hemagglutinin subtypes and viruses.

Prospects for immune escape

The remarkable transformation to the fusogenic state includes repacking of the central helices of three HA2 protomers to form a new triple-helical bundle, in which residues 34–37 form an N-terminal cap, and the creation of C-terminal arms that extend to the N terminus of the new bundle[37]. It is straightforward to model the locations of the F10 epitope residues in this model of the fusogenic state (**Supplementary Note 1** online). All eight epitope residues, which were fully exposed in the neutral pH structure, become either part of the new hydrophobic bundle core ($Thr41_2$, $Ile45_2$, $Val52_2$ and $Ile56_2$) or they make networks of hydrogen bonds with the C-terminal arms and other elements that stabilize the new bundle ($Lys\ 38_2$, $Gln42_2$, $Thr49_2$ and $Asn53_2$). The requirement for adopting two entirely different conformations, each with a distinct hydrophobic core and hydrogen-bonding network may place powerful evolutionary constraints on the sequence of the helix, as evidenced by the almost complete lack of genetic drift within helix αA among the 16 hemagglutinin subtypes.

To test this hypothesis, we attempted to select neutralization-escape mutants. We propagated VN/04 (H5N1) virus in MDCK cells for 72 h in the presence of 40 μg ml^{-1} of each of the 3 nAbs as well as a murine antibody, 22F, that targets the receptor binding head. Following three *in vitro* passages, we readily isolated a mutant VN04 virus (K193E) that was resistant to 22F. In contrast, we failed to identify any viruses resistant to any of our three IgG1s (D8, F10 or A66). Although these experiments cannot prove that escape mutants with unimpaired viral fitness will never arise, they clearly support the notion that the pocket is more refractory than epitopes in the head. Notwithstanding, if such mutants should arise, we can use our *in vitro* approach to find new reactive nAbs, or further engineer the existing nAbs to have even broader spectrum reactivity[38].

DISCUSSION

Before the present study, the vast majority of nAbs isolated against influenza A virus have targeted the receptor binding head and lacked broad cross-neutralizing activity. However, a murine nAb, termed C179 (ref. 39), was positively selected on the basis of its cross-neutralization properties (of H1 and H2 subtypes) and was subsequently shown to neutralize H5, but not group 2, subtypes[39,40] (**Supplementary Note 2** online). Moreover, C179 was shown to block membrane fusion rather than cell attachment and to protect mice against viral challenge[41], although a detailed mechanism was not reported. We compared the activities of C179 and F10 and found that both showed similar binding toward H5. We also found that F10 efficiently competed with C179 for binding to H5, but not vice versa (**Supplementary Fig. 9** online). Furthermore, the point mutant $V52_2E$ abrogated binding to both antibodies, whereas $T318_1K$ affected only C179 binding. These results suggest that F10 and C179 have partially overlapping epitopes and that their modes of action are similar.

The manner in which hemagglutinin was presented to the antibody phage-display library in this study seems to have been crucial in our success, because similar attempts to isolate broadly nAbs using cell-surface expressed hemagglutinin showed only partial success against H5, and most antibodies recognized linear epitopes[42]. As noted above, we repeatedly isolated nAbs that use the same VH germline gene (*IGHV1-69* or '*VH1-69*'). One published study pointed out that this is the only VH gene that consistently encodes two hydrophobic residues

at the tip of its CDR-H2 loop[43]; indeed, it is the only germline gene to encode a phenylalanine at this position, which makes several crucial interactions with H5. Moreover, the 'type 2' H2 loop, which is long and compact, is predicted to occur in only 4 out of the ~50 human germline genes. These factors may explain at least in part the ability of nAbs derived from this germline gene to cross-react with viral epitopes through their unusual ability to bind to conserved hydrophobic pockets. Such pockets are likely to have an important function and for this reason they are often cryptic in the unactivated state of the antigen. For example, *VH1-69* is the predominant gene used by a group of CD4-induced nAbs raised against the HIV-1 surface glycoprotein, gp120, where the pocket is part of a conserved co-receptor binding site that is exposed only transiently upon binding to its primary receptor, CD4 (ref. 43). Similarly, an antibody raised against the HIV gp41 trimeric 'inner-core' fusion protein intermediate uses the hydrophobic tip of its VH1-69 CDR-H2 loop to insert into a conserved hydrophobic pocket that blocks further assembly to the fusion-competent six-helix structure[44]. *In vivo*, B cells carrying the *VH1-69* gene are the primary mediators of innate defense against HCV infection, generating antibodies against its membrane-fusion glycoprotein, E2 (ref. 45), although the epitope and mode of action have not been determined. Notably, as we found here, *VH1-69* is not the only germline gene that is suitable for achieving neutralization in a similar manner. Another recent example is a nAb against the Ebola virus surface glycoprotein, KZ52, which uses the *VH3-21* germline gene[46]. However, their common ability to lock viral envelope proteins into a nonfusogenic conformation suggests a general strategy for broad-spectrum and/or potent viral neutralization.

Recent work using immune-based phage-display libraries generated from B cell populations of patients who survived H5N1 infection resulted in the isolation of three human nAbs that neutralized both H1 and H5 viral strains. The authors postulated that the reason for survival was an effective humoral immune response mediated by such nAb-generating B cells *in vivo*[47], although no control populations were studied. Analysis of their data (**Supplementary Note 3** online) indicates that the antibodies are also derived from the *VH1-69* germline gene and share other key characteristics, including the methionine-phenylalanine pair in CDR-H2 and a tyrosine at the tip of CDR-H3. Thus it would seem, at least in this case, that our non-immune (H5-naive) donor library approach generated antibodies with characteristics similar to those found using immunized donor–based phage-display libraries derived from H5N1 survivors.

Why broad-spectrum nAbs similar to those identified in our study are not similarly generated and expanded during successive rounds of influenza infection and repeated vaccination is not known (**Supplementary Note 4** online), and this question warrants further investigation. It is unlikely that the F10 epitope provokes self-tolerance mechanism(s) via auto-antigen mimicry[48] (**Supplementary Note 5** online). Rather, we hypothesize that an immunodominant antibody response to the highly exposed globular head may overwhelm the antibody response to the F10 epitope, although it remains possible that other immune exclusion mechanism(s) may preclude natural antibody responses against it. It is not surprising that many viruses are highly adept at keeping their most crucial (and conserved) determinants of pathogenesis cryptic, in which case subunit-based vaccines, using properly presented fragments of F10 or F10-like epitopes, may offer distinct advantages over whole virus–based approaches to induce broad spectrum nAbs *in vivo*[49,50].

In summary, we have used *in vitro* methodologies to isolate a family of high-affinity broad-spectrum human nAbs against hemagglutinin that show potent *in vitro* and *in vivo* efficacy against both highly pathogenic H5N1 and H1N1 viruses. We show that they inhibit the post-attachment fusion process by recognizing a highly conserved epitope within the stem region of hemagglutinin at a point where key elements of the conformational change are brought into close apposition. Our initial experiments suggest that this region is recalcitrant to the generation of escape mutants. The prospects for their use for passive immunotherapy would therefore seem to be excellent, either alone or in combination with small-molecule inhibitors (**Supplementary Note 6** online). Finally, our structural work pinpoints the reasons why group 2 hemagglutinins do not bind the nAbs described here: despite surface sequence similarities, they form a structurally distinct group, but one that is also highly conserved and therefore may be amenable to a similar panning discovery approach.

Note added in proof: Throsby et al.[51] recently identified human nAbs that recognize a broad range of group 1 influenza A viruses with similar VH1-69 germline gene usage.

METHODS

Crystallization of the H5–F10 complex. We generated H5–F10 complexes by incubating the two purified components with an excess of F10 (**Supplementary Methods** online) and isolated them by Superdex 200 in Tris-buffered saline (TBS) buffer. Peak fractions were pooled and concentrated to ~11 mg ml^{-1}. We examined the integrity of the H5 trimer using gel filtration and SDS-PAGE. Crystals grew at 22 °C by equilibrating equal volumes of protein and reservoir solution (12.5% PEG 1K (w/v), 25% ethylene glycol (w/v), 100 mM Tris, pH 8.5) using the hanging drop vapor diffusion technique.

Data collection, structure determination and refinement. We collected diffraction data from crystals that were flash frozen at 100 K in the reservoir

Table 1 Data collection and refinement statistics for H5–F10

	Native H5–F10
Data collection	
Space group	*C*2
Cell dimensions	
a, *b*, *c* (Å)	205, 119, 339
α, β, γ (°)	90, 99.6, 90
Resolution (Å)	3.2 (3.28–3.20)*
R_{merge}	0.13 (0.81)
$I / \sigma I$	9.5 (2.0)
Completeness (%)	85 (68)
Redundancy	4.5 (4.5)
Refinement	
Resolution (Å)	50–3.2 (3.28–3.20)
No. reflections	106,885
R_{work} / R_{free}	0.23 (0.32)/0.29 (0.38)
No. atoms	
Protein	34,573
Carbohydrate	402
Water	0
B-factors	
Protein	83.5
Carbohydrate	123.7
r.m.s. deviations	
Bond lengths (Å)	0.010
Bond angles (°)	1.31

A single crystal was used for both structure determination at 3.2-Å resolution and refinement.
*Values in parentheses are for highest-resolution shell.

buffer at the Stanford Synchrotron Radiation Laboratory beamline 9.2, set at a wavelength of 1.0 Å and processed with XDS[52] and HKL2000 (ref. 53). The structure was solved at 3.2-Å resolution by molecular replacement with PHASER using the structures of H5 (A/Vietnam/1194/04; PDB 2IBX) and a homology model of F10 based on the structure of SARS nAb 80R (PDB 2GHW)[54,55] as starting models. The asymmetric unit contains two H5 trimers and three F10 molecules per trimer and was refined using REFMAC5 (ref. 56) with simulated annealing in CNS and manual rebuilding with Coot[57] and Xtalview[58]. The final maps are of high quality, and key features such as the F10 CDR loops and interfacial residues are unambiguous and consistent in the six copies. The final model includes 503, 503, 503, 497, 497 and 497 residues for the six independent copies of H5; 235, 235, 236, 233, 234 and 234 residues for the six F10scFvs; 24 *N*-acetyl-D-glucosamine and six β-D-mannose units, but no water molecules. The R_{free} is 0.29 with excellent geometry as assessed with PROCHECK[59] and Rampage (**Table 1**): residues in the favored, allowed and outlier regions are 90.0%, 9.5% and 0.5%, respectively.

Phage-display library selection. We produced recombinant trimeric H5-VN04 ectodomain as for crystallization studies except that we did not use furin co-infection to ensure complete activation. Antibodies were identified by two rounds of selection of a 27 billion–membered human scFv phage-display library against recombinant trimeric H5 immobilized on Immunotube (Nunc), followed by ELISA screening. We identified ten unique anti-H5 antibodies by sequence analysis of 97 H5-positive clones out of 392 clones screened.

Plaque reduction assay. H5-VN04, H5-IN05 or A/Netherland/219/03 (H7N7) (H7-NL03) viruses (10,000 plaque forming units (p.f.u.)) were incubated with anti-H5 scFv-Fcs at three different concentrations (1 μg ml^{-1}, 10 μg ml^{-1}or 100 μg ml^{-1}) at 37 °C for 30 min. We diluted the virus-antibody mixture logarithmically and transferred the dilutions onto MDCK cell monolayers in 12-well plates, which we then incubated at 37 °C for 1 h. The cells were then washed and overlaid with agar. After 4 d of incubation, we discarded the overlay and the plaques were visualized by crystal violet staining.

Microneutralization assay. We carried out the assay as described[60]. Briefly, we mixed 100 $TCID_{50}$ (median tissue culture infectious doses) of virus in equal volume with two-fold serial dilutions of antibody stock solution (0.1 mg ml^{-1}) in 96-well plates and incubated them for 1 h at 37 °C. Indicator MDCK cells (1.5×10^4 cells per well) were added to the plates, followed by incubation at 37 °C for 20 h. To establish the endpoint, we washed the cell monolayers with PBS, fixed the cells in acetone and detected viral antigen by indirect ELISA with a mAb against influenza A NP (A-3, Accurate).

Viral binding inhibition assay. We incubated 0.5×10^6 293T cells with H5-TH04–pseudotyped HIV viruses (~500 ng of p24) in the presence of anti-H5 nAbs or control mAbs, or in the absence of antibodies, in PBS buffer containing 0.5% (w/v) BSA and 0.02% (w/v) NaN_3 at 4 °C. After 1 h of incubation, cells were spun down, and the supernatants were tested for p24 levels using an HIV-1 $p24^{CA}$ capture ELISA kit (National Cancer Institute, US National Institutes of Health) to quantify unbound virus. Cells were then washed once or twice and lysed to quantify the cell-bound virus using the same method.

Cell fusion inhibition assay. We transfected HeLa cells, ~90% confluent in six-well plates, with pcDNA3.1-H5-TH04 plasmid (3 μg total DNA per well) using lipofectamine 2000 (Invitrogen). After ~30 h of transfection, the culture medium was supplemented with 1 ml of anti-H5 or control mAbs for 1–2 h, and cells were then washed and incubated with low-pH fusion buffer (150 mM NaCl plus 10 mM HEPES, adjusted to pH 5.0) for 4–5 min. Cells were then returned to the standard culture medium for 2–3 h at 37 °C, and finally fixed with 0.25% (v/v) glutaraldehyde and stained with 0.1% (w/v) crystal violet. Photomicrographs were taken at 10× magnification.

Prophylactic and therapeutic efficacy studies in mice. We used female 8–10 weeks old BALB/c mice in all experiments. Mice were weighed on the day of virus challenge and then daily for 2 weeks. We used body weight as the clinical endpoint; mice with body weight loss ≥25% of pre-infection values were euthanized. Animal studies were conducted as per the approved Institutional Animal Care and Use Committee protocols.

For the prophylactic efficacy study, three human nAbs (D8-IgG1, F10-IgG1 and A66-IgG1) or control human mAb 80R-IgG1 (ref. 18) at 2.5 mg kg^{-1} or 10 mg kg^{-1} were administered into four groups of five mice each by intraperitoneal injection in a 0.5 ml volume. At 1 h after mAb administration, two groups of mice were challenged with H5-VN04 and two groups with H5-HK97 intranasal inoculation with 10 MLD_{50} in 50 μl volumes per mouse. Mice were observed and weighed daily for 2 weeks after infection. Analogous studies were performed to evaluate the protective efficacy of the nAbs against A/Puerto Rico/8/1934 (H1N1) or A/WSN/1933 (H1N1) viruses.

For the post-exposure therapy efficacy study, the experimental design recapitulates the prophylaxis study, with the following exceptions. We first inoculated 12 groups of ten mice intranasally with 10 MLD_{50} of VN04. At 24 h, 48 h and 72 h after H5-VN04 infection, the mice received intraperitoneal injections of 15 mg kg^{-1} body weight of one of the nAbs or control (80R).

Accession codes. Protein Data Bank: Coordinates and structure factors for the H5–F10 complex have been deposited with accession code 3FKU.

Note: Supplementary information is available on the Nature Structural & Molecular Biology website.

ACKNOWLEDGMENTS

We thank J. Appleton (Cornell University) for the gift of mouse mAbs against H5N1, 17A2.1.2 and 22F; A. Klimov (CDC) and A. Balish (CDC) for providing ferret antiserum and virus sequences; R. Webster (St. Jude Children's Research Hospital) for H11N9, H13N6 and H16N3; L. Quynh Mai (National Institute of Hygiene and Epidemiology, Vietnam Ministry of Health) for H5N1; W. Lim (Hong Kong Department of Health) for H5N1 and H9N2, as well as E. Sedyaningsih, T. Soendoro (National Institute of Health Research and Development, Indonesian Ministry of Health) for H5N1 specimens; P. Palese (Mount Sinai School of Medicine) for pCAGGS-H1(SC) plasmid encoding the full-length hemagglutinin protein of H1-SC1918; M. Farzan (New England Primate Research Center, Harvard Medical School) for pCAGGS-H1 (PR) plasmid encoding the hemagglutinin protein of H1-PR34 and X. Yang (Beth Israel Deaconess Medical Center, Harvard Medical School) for pCAGGS-H7 (FPV) encoding H7-FP34 hemagglutinin; and R. Fuller (University of Michigan) for furin cDNA. We thank W. Yuan and W. Li for helpful discussions and Y. Lin for assistance in crystallization and critical discussion. We thank the US National Institutes of Health (NIH) and the Department of Energy (DOE) for access to the Stanford Synchrotron Radiation Facility and the facility staff for assistance in X-ray data collection. Molecular graphics images were produced using the UCSF Chimera package from the Resource for Biocomputing, Visualization, and Informatics at the University of California, San Francisco (supported by NIH P41 RR-01081). This work was supported by NIH (U01-AI074518-01) to W.A.M. and in part by NIH (P01-AI055789) to R.C.L.

AUTHOR CONTRIBUTIONS

In the DFCI team, J.S. and A.M. constructed H5-TH04 hemagglutinin; J.S. and D.A. performed phage-display antibody library selections and screening for antibodies by ELISA, FACS and pseudovirus-neutralization assays; J.S., M.A. and T.H. carried out epitope mapping using mutagenesis and FACS analysis; J.S., D.A. and M.A. purified antibodies; J.S. and A.Y. analyzed kinetics of antibody binding with hemagglutinin protein; J.S. performed hemagglutinin subtype cross-binding and neutralization assays, pseudovirus binding and fusion inhibition assay; J.S. and W.A.M. designed the study, analyzed data and wrote the sections about these studies. In the BIMR team, R.C.L. supervised all of the work; G.W. and G.C. cloned and expressed recombinant H5 for antibody panning and crystallization. W.C.H. expressed F10 scFv and crystallized the F10–HA0 complex; W.C.H., E.S. and B.S. collected diffraction data and solved and refined the structure; L.A.B. supervised cloning and expression; W.C.H., L.A.B. and R.C.L. wrote sections about these studies. In the CDC team, S.P., L.C., H.W., N.J.C. and R.O.D. designed the study and performed animal studies as well as virology studies with wild-type viruses; R.O.D wrote sections of these studies; J.S., R.O.D., R.C.L. and W.A.M. finalized the paper. All authors commented on the manuscript. The findings and conclusions in this report are those of the authors and do not necessarily represent the views of the Centers for Disease Control and Prevention or the Agency for Toxic Substances and Disease Registry.

Published online at http://www.nature.com/nsmb/
Reprints and permissions information is available online at http://npg.nature.com/reprintsandpermissions/

1. WHO. Factsheet 211: influenza. *World Health Organization* 〈http://www.who.int/mediacentre/factsheets/2003/fs211/en/〉 (2003).
2. Webster, R.G. 1918 Spanish influenza: the secrets remain elusive. *Proc. Natl. Acad. Sci. USA* **96**, 1164–1166 (1999).
3. de Wit, E. & Fouchier, R.A. Emerging influenza. *J. Clin. Virol.* **41**, 1–6 (2008).
4. WHO. Global influenza surveillance. *World Health Organization* 〈http://www.who.int/csr/disease/influenza/influenzanetwork/en/index.html〉 (2008).
5. Carrat, F. & Flahault, A. Influenza vaccine: the challenge of antigenic drift. *Vaccine* **25**, 6852–6862 (2007).
6. Cinatl, J. Jr, Michaelis, M. & Doerr, H.W. The threat of avian influenza A (H5N1). Part IV: development of vaccines. *Med. Microbiol. Immunol.* **196**, 213–225 (2007).
7. Subbarao, K. & Luke, C. H5N1 viruses and vaccines. *PLoS Pathog.* **3**, e40 (2007).
8. Leroux-Roels, I. *et al.* Broad clade 2 cross-reactive immunity induced by an adjuvanted clade 1 rH5N1 pandemic influenza vaccine. *PLoS ONE* **3**, e1665 (2008).
9. Baras, B. *et al.* Cross-Protection against lethal H5N1 challenge in ferrets with an adjuvanted pandemic influenza vaccine. *PLoS ONE* **3**, e1401 (2008).
10. de Jong, M.D. *et al.* Oseltamivir resistance during treatment of influenza A (H5N1) infection. *N. Engl. J. Med.* **353**, 2667–2672 (2005).
11. WHO. Clinical management of human infection with avian influenza A (H5N1) virus. *World Health Organization* 〈http://www.who.int/csr/disease/avian_influenza/guidelines/ClinicalManagement07.pdf〉 (2007).
12. Wright, P., Neumann, G. & Kawaoka, Y. Orthomyxoviruses. in *Fields Virology* Vol. 2 (eds. Knipe, D., Howley, P., Griffin, D., Lamb, R. & Martin, M.) 1692–1740 (Lippincott Williams & Wilkins, Philadelphia, PA, 2006).
13. Fauci, A.S. Pandemic influenza threat and preparedness. *Emerg. Infect. Dis.* **12**, 73–77 (2006).
14. Marasco, W.A. & Sui, J. The growth and potential of human antiviral monoclonal antibody therapeutics. *Nat. Biotechnol.* **25**, 1421–1434 (2007).
15. WHO. Antigenic and genetic characteristics of H5N1 viruses and candidate H5N1 vaccine viruses developed for potential use as pre-pandemic vaccines. *World Health Organization* 〈http://www.who.int/csr/disease/avian_influenza/guidelines/summaryH520070403.pdf〉 (2007).
16. World Health Organization Global Influenza Program Surveillance Network. Evolution of H5N1 avian influenza viruses in Asia. *Emerg. Infect. Dis.* **11**, 1515–1521 (2005).
17. Stevens, J. *et al.* Structure and receptor specificity of the hemagglutinin from an H5N1 influenza virus. *Science* **312**, 404–410 (2006).
18. Sui, J. *et al.* Potent neutralization of severe acute respiratory syndrome (SARS) coronavirus by a human mAb to S1 protein that blocks receptor association. *Proc. Natl. Acad. Sci. USA* **101**, 2536–2541 (2004).
19. Skehel, J.J. & Wiley, D.C. Receptor binding and membrane fusion in virus entry: the influenza hemagglutinin. *Annu. Rev. Biochem.* **69**, 531–569 (2000).
20. Kida, H., Yoden, S., Kuwabara, M. & Yanagawa, R. Interference with a conformational change in the haemagglutinin molecule of influenza virus by antibodies as a possible neutralization mechanism. *Vaccine* **3**, 219–222 (1985).
21. Ha, Y., Stevens, D.J., Skehel, J.J. & Wiley, D.C. H5 avian and H9 swine influenza virus haemagglutinin structures: possible origin of influenza subtypes. *EMBO J.* **21**, 865–875 (2002).
22. Chothia, C. *et al.* Structural repertoire of the human VH segments. *J. Mol. Biol.* **227**, 799–817 (1992).
23. Samanta, U., Pal, D. & Chakrabarti, P. Packing of aromatic rings against tryptophan residues in proteins. *Acta Crystallogr. D Biol. Crystallogr.* **55**, 1421–1427 (1999).
24. Weis, W.I., Brunger, A.T., Skehel, J.J. & Wiley, D.C. Refinement of the influenza virus hemagglutinin by simulated annealing. *J. Mol. Biol.* **212**, 737–761 (1990).
25. Pal, D. & Chakrabarti, P. Non-hydrogen bond interactions involving the methionine sulfur atom. *J. Biomol. Struct. Dyn.* **19**, 115–128 (2001).
26. Champ, P.C. & Camacho, C.J. FastContact: a free energy scoring tool for protein-protein complex structures. *Nucleic Acids Res.* **35**, W556–W560 (2007).
27. Stevens, J. *et al.* Structure of the uncleaved human H1 hemagglutinin from the extinct 1918 influenza virus. *Science* **303**, 1866–1870 (2004).
28. Daniels, R.S. *et al.* Fusion mutants of the influenza virus hemagglutinin glycoprotein. *Cell* **40**, 431–439 (1985).
29. Thoennes, S. *et al.* Analysis of residues near the fusion peptide in the influenza hemagglutinin structure for roles in triggering membrane fusion. *Virology* **370**, 403–414 (2008).
30. Earp, L.J., Delos, S.E., Park, H.E. & White, J.M. The many mechanisms of viral membrane fusion proteins. *Curr. Top. Microbiol. Immunol.* **285**, 25–66 (2005).
31. Barbey-Martin, C. *et al.* An antibody that prevents the hemagglutinin low pH fusogenic transition. *Virology* **294**, 70–74 (2002).
32. Russell, R.J. *et al.* H1 and H7 influenza haemagglutinin structures extend a structural classification of haemagglutinin subtypes. *Virology* **325**, 287–296 (2004).
33. Fouchier, R.A. *et al.* Characterization of a novel influenza A virus hemagglutinin subtype (H16) obtained from black-headed gulls. *J. Virol.* **79**, 2814–2822 (2005).
34. Gamblin, S.J. *et al.* The structure and receptor binding properties of the 1918 influenza hemagglutinin. *Science* **303**, 1838–1842 (2004).
35. Yamada, S. *et al.* Haemagglutinin mutations responsible for the binding of H5N1 influenza A viruses to human-type receptors. *Nature* **444**, 378–382 (2006).
36. Ha, Y., Stevens, D.J., Skehel, J.J. & Wiley, D.C. X-ray structure of the hemagglutinin of a potential H3 avian progenitor of the 1968 Hong Kong pandemic influenza virus. *Virology* **309**, 209–218 (2003).
37. Chen, J., Skehel, J.J. & Wiley, D.C. N- and C-terminal residues combine in the fusion-pH influenza hemagglutinin HA_2 subunit to form an N cap that terminates the triple-stranded coiled coil. *Proc. Natl. Acad. Sci. USA* **96**, 8967–8972 (1999).
38. Sui, J. *et al.* Broadening of neutralization activity to directly block a dominant antibody-driven SARS-coronavirus evolution pathway. *PLoS Pathog.* **4**, e1000197 (2008).
39. Okuno, Y., Isegawa, Y., Sasao, F. & Ueda, S. A common neutralizing epitope conserved between the hemagglutinins of influenza A virus H1 and H2 strains. *J. Virol.* **67**, 2552–2558 (1993).
40. Smirnov, Y.A. *et al.* An epitope shared by the hemagglutinins of H1, H2, H5, and H6 subtypes of influenza A virus. *Acta Virol.* **43**, 237–244 (1999).
41. Smirnov, Y.A., Lipatov, A.S., Gitelman, A.K., Claas, E.C. & Osterhaus, A.D. Prevention and treatment of bronchopneumonia in mice caused by mouse-adapted variant of avian H5N2 influenza A virus using monoclonal antibody against conserved epitope in the HA stem region. *Arch. Virol.* **145**, 1733–1741 (2000).
42. Lim, A.P. *et al.* Neutralizing human monoclonal antibody against H5N1 influenza HA selected from a Fab-phage display library. *Virol. J.* **5**, 130 (2008).
43. Huang, C.C. *et al.* Structural basis of tyrosine sulfation and VH-gene usage in antibodies that recognize the HIV type 1 coreceptor-binding site on gp120. *Proc. Natl. Acad. Sci. USA* **101**, 2706–2711 (2004).
44. Luftig, M.A. *et al.* Structural basis for HIV-1 neutralization by a gp41 fusion intermediate-directed antibody. *Nat. Struct. Mol. Biol.* **13**, 740–747 (2006).
45. Chan, C.H., Hadlock, K.G., Foung, S.K. & Levy, S. V_H1–*69* gene is preferentially used by hepatitis C virus-associated B cell lymphomas and by normal B cells responding to the E2 viral antigen. *Blood* **97**, 1023–1026 (2001).
46. Lee, J.E. *et al.* Structure of the Ebola virus glycoprotein bound to an antibody from a human survivor. *Nature* **454**, 177–182 (2008).
47. Kashyap, A.K. *et al.* Combinatorial antibody libraries from survivors of the Turkish H5N1 avian influenza outbreak reveal virus neutralization strategies. *Proc. Natl. Acad. Sci. USA* **105**, 5986–5991 (2008).
48. Scherer, E.M., Zwick, M.B., Teyton, L. & Burton, D.R. Difficulties in eliciting broadly neutralizing anti-HIV antibodies are not explained by cardiolipin autoreactivity. *AIDS* **21**, 2131–2139 (2007).
49. Selvarajah, S. *et al.* Focused dampening of antibody response to the immunodominant variable loops by engineered soluble gp140. *AIDS Res. Hum. Retroviruses* **24**, 301–314 (2008).
50. Scheerlinck, J.P. *et al.* Redistribution of a murine humoral immune response following removal of an immunodominant B cell epitope from a recombinant fusion protein. *Mol. Immunol.* **30**, 733–739 (1993).
51. Throsby, M. *et al.* Heterosubtypic neutralizing monoclonal antibodies cross-protective against H5N1 and H1N1 recovered from human IgM^+ memory B cells. *PLoS ONE* **3**, e3942 (2008).
52. Kabsch, W. Automatic processing of rotation diffraction data from crystals of initially unknown symmetry and cell constants. *J. Appl. Cryst.* **26**, 795–800 (1993).
53. Otwinowski, Z.O. & Minor, W. Processing of X-ray diffraction data collected in oscillation mode. *Methods Enzymol.* **276**, 307–326 (1997).
54. Hwang, W.C. *et al.* Structural basis of neutralization by a human anti-severe acute respiratory syndrome spike protein antibody, 80R. *J. Biol. Chem.* **281**, 34610–34616 (2006).
55. Rodriguez, R., Chinea, G., Lopez, N., Pons, T. & Vriend, G. Homology modeling, model and software evaluation: three related resources. *Bioinformatics* **14**, 523–528 (1998).
56. Murshudov, G.N., Vagin, A.A. & Dodson, E.J. Refinement of macromolecular structures by the maximum-likelihood method. *Acta Crystallogr. D Biol. Crystallogr.* **53**, 240–255 (1997).
57. Emsley, P. & Cowtan, K. Coot: model-building tools for molecular graphics. *Acta Crystallogr. D Biol. Crystallogr.* **60**, 2126–2132 (2004).
58. McRee, D.E. A visual protein crystallographic software system for X11/Xview. *J. Mol. Graph.* **10**, 44–46 (1992).
59. Laskowski, R.A., MacArthur, M.W., Moss, D.S. & Thornton, J.M. PROCHECK: a program to check the stereochemical quality of protein structures. *J. Appl. Cryst.* **26**, 283–291 (1993).
60. Rowe, T. *et al.* Detection of antibody to avian influenza A (H5N1) virus in human serum by using a combination of serologic assays. *J. Clin. Microbiol.* **37**, 937–943 (1999).
61. Bullough, P.A., Hughson, F.M., Skehel, J.J. & Wiley, D.C. Structure of influenza haemagglutinin at the pH of membrane fusion. *Nature* **371**, 37–43 (1994).

Supplementary Information

Structural and Functional Bases for Broad-Spectrum Neutralization of Avian and Human Influenza A Viruses

Jianhua Sui [1], William C. Hwang [2], Sandra Perez [3], Ge Wei [2], Daniel Aird [1], Li-mei Chen [3], Eugenio Santelli [2], Boguslaw Stec [2], Greg Cadwell [2], Maryam Ali [1], Hongquan Wan [3], Akikazu Murakami [1], Anuradha Yammanuru [1], Thomas Han [1], Nancy J. Cox[3], Laurie A. Bankston [2], Ruben O. Donis [3], Robert C. Liddington [2] and Wayne A. Marasco [1]

[1]Department of Cancer Immunology & AIDS, Dana-Farber Cancer Institute; Department of Medicine, Harvard Medical School, 44 Binney St. JFB 826, Boston, MA 02115, USA

[2]Infectious and Inflammatory Disease Center, Burnham Institute for Medical Research, 10901 North Torrey Pines Road, La Jolla, CA 92037, USA.

[3]Influenza Division, Centers for Disease Control and Prevention, National Center for Immunization and Respiratory Diseases, 1600 Clifton Road - Mail Stop G-16, Atlanta, GA 30333, USA.

Nature Structural & Molecular Biology: doi:10.1038/nsmb.1566

Supplementary Fig. 1

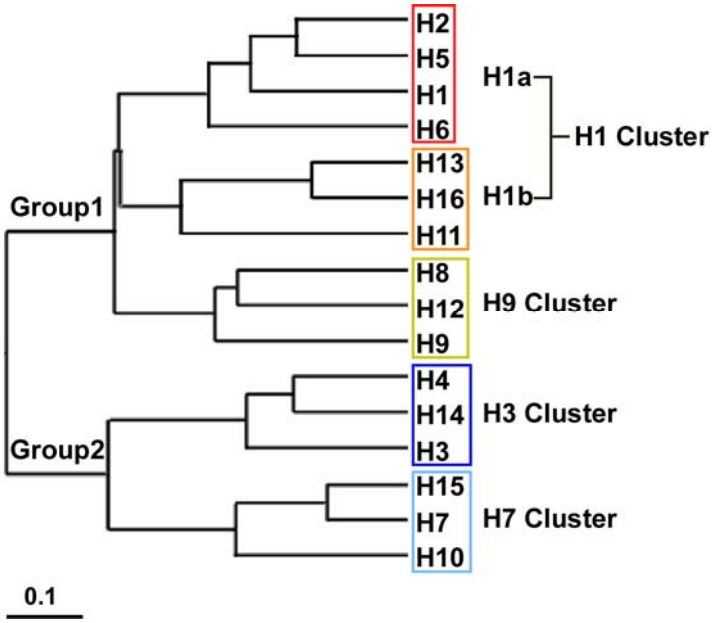

Fig. S1. Phylogenetic relationships among HA subtypes. Phylogenetic tree of the 16 HA subtypes of influenza A viruses based on amino-acid sequences. Four clusters of HA subtypes are shaded in different colors. The sequences used for analysis were:
H1 (A/South Carolina/1/1918),H2 (A/Japan/305/1957),
H3 (A/Aichi/2/1968), H4 (A/duck/Czechoslovakia/56),
H5 (A/VietNam1203/2004), H6 (A/chicken/California/431/00),
H7 (A/Netherland/219/03), H8 (A/turkey/Ontario/6118/68),
H9 (A/swine/HK/9/98), H10 (A/chicken/Germany/N49),
H11 (A/duck/England/56), H12 (A/duck/Alberta/60/76),
H13 (A/gull/Maryland/704/77), H14 (A/mallard/Astrakhan/263/1982),
H15 (A/shearwater/West Australia/2576/79)
and H16 (A/black-headed gull/Sweden/2/99).

Supplementary Fig. 2

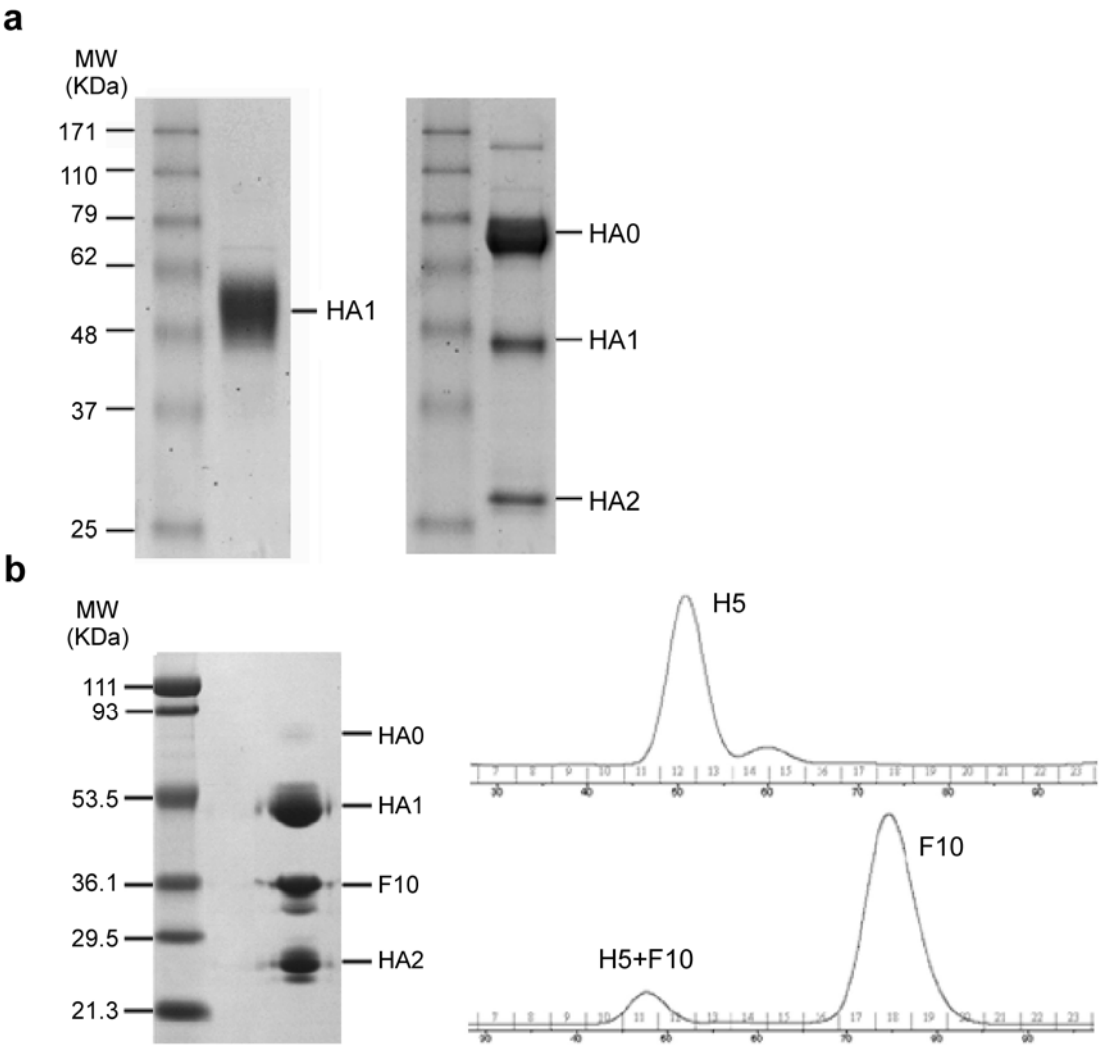

Fig. S2. SDS-PAGE and gel filtration analysis of HA proteins. (a) HA1-specific antibody 2A was obtained from a separate HA1-targeted selection against the HA1 (residues 11-325) fragment of H5-TH04 (left panel). H5 HA (H5-VN04 strain) used for library selection is shown in the right panel (the majority is uncleaved HA0). **(b)** H5-VN04 (H5) and scFv F10 complex. HA0 was fully cleaved into HA1 and HA2 by co-expression with furin (left panel). Complexes were formed by first mixing H5 and F10 at a molar ratio of 1:10, and then purified by gel filtration.

Supplementary Fig. 3

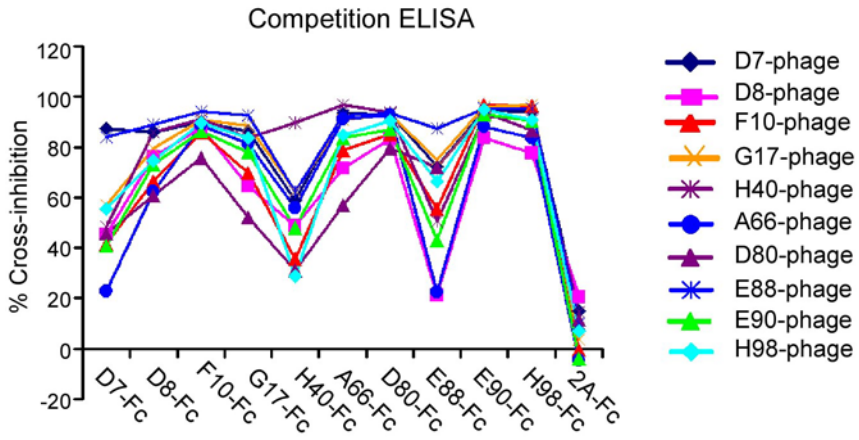

Fig. S3. Competition ELISA assay between soluble and phage-bound nAbs. All anti-H5 nAbs cross-competed, consistent with an overlapping epitope, while anti-HA1 ("2A-Fc") did not. 10^{12} pfu of anti-H5 phage-scFv-Fcs were mixed with 5 μg/mL of soluble nAbs and added to H5-VN04-coated plates, washed, and followed by HRP-anti-M13 to detect phage-bound H5**.**

Supplementary Fig.4

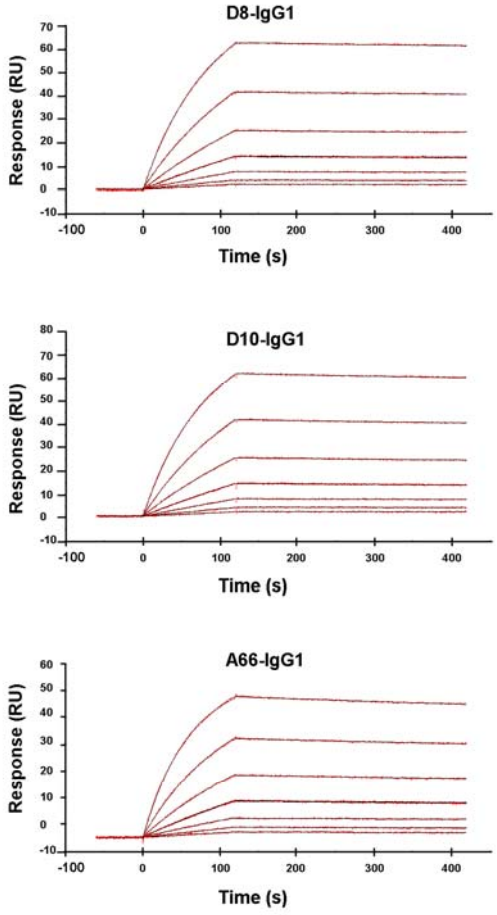

$$A + B \underset{kd}{\overset{ka}{\rightleftharpoons}} AB$$

	ka (M^{-1} s^{-1} x 10^5)	kd (s^{-1}x10^{-4})	K_D (pM)
D8-IgG1	5.98±0.08	0.88±0.11	148±19
F10-IgG1	6.52±0.92	0.84±0.19	130±28
A66-IgG1	7.75±0.63	1.80±0.31	233±47

Fig. S4. Kinetic and thermodynamic characterization of the binding of H5 HA to nAbs D8, F10 and A66-IgG1s. nAbs were captured on a CM4 chip via anti-human IgG1; trimeric H5 (H5-VN04) at various concentrations (20, 10, 5, 2.5, 2.5, 1.25, 0.625 nM) was injected over the chip surface. Binding kinetics were evaluated using a 1:1 Langmuir binding model. The recorded binding curves (with blank reference subtracted) and the calculated curves are closely superimposable. Each *ka, kd* and K_D value represents the mean and standard error of three experiments.

Supplementary Fig. 5

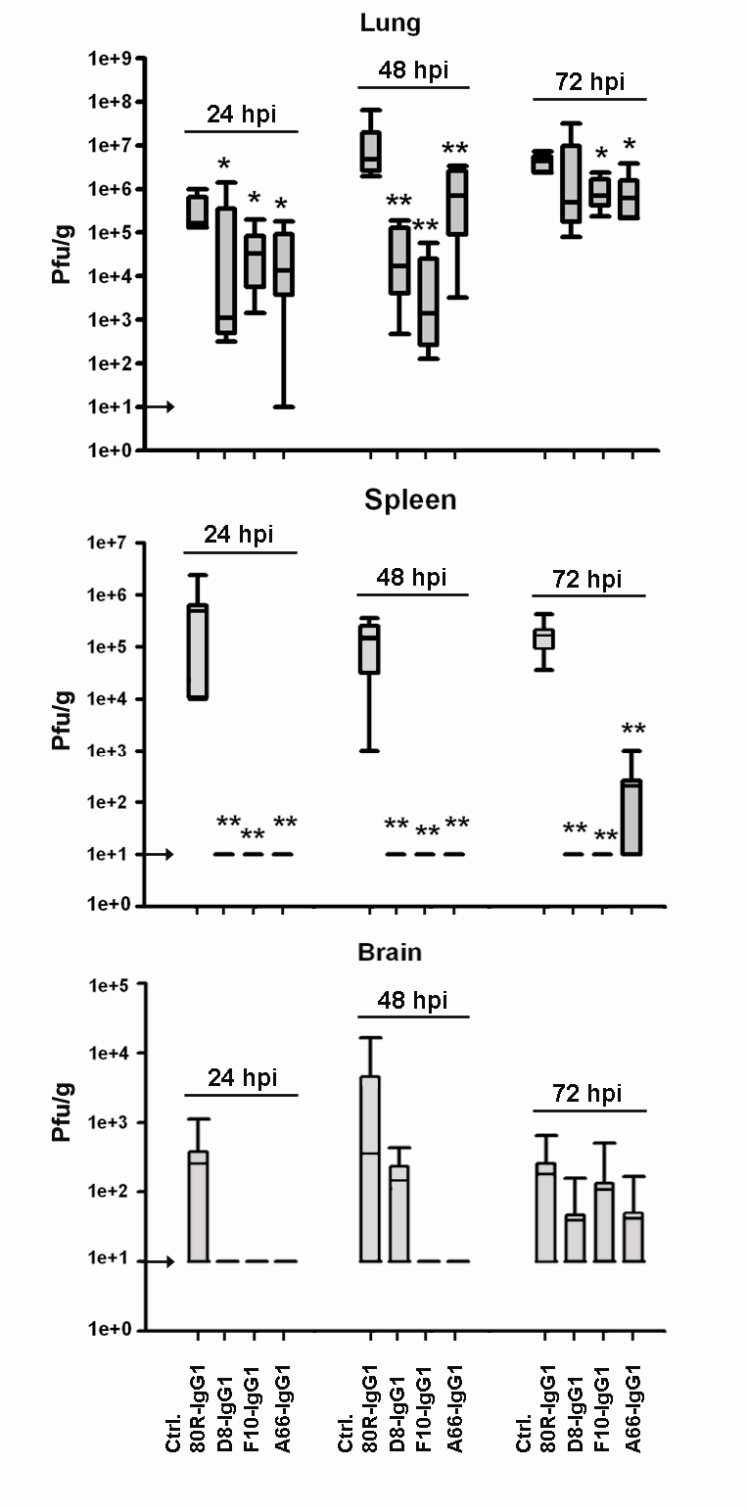

Fig. S5. Viral titers in lung, spleen and brain of mice treated with anti-H5 nAbs after H5-VN04 challenge. BALB/c mice (n=5) were treated by i.p. injection of 15 mg/kg of mAb at 24, 48 or 72 hrs after i.n. infection with 10 MLD_{50} of H5-VN04 as described in Fig 3 of the main text. Viral titers were determined at 96 hpi either in lungs, as an indicator of inhibition of local replication, or in spleen and brain, indicative of the systemic spread that is characteristic of H5N1 infection. The nAbs mediated a significant suppression of viral replication in lungs when given within 48 hours of challenge. Notably, two of the nAbs, D8 and F10, also showed significant antiviral effect when given at 72 hpi. The impact of nAb therapy on systemic spread was demonstrated by ≥ 1000-fold suppression of virus spread to the spleen even when the three nAbs were given within 72 hpi. Systemic virus spread to the brain was low in control animals, obscuring statistically significant effect of nAb treatment, but still showing a general pattern of suppression. Data are displayed in box-and-whiskers form in which the box extends from the 25^{th} to the 75^{th} percentile, with a horizontal line at the median. Whiskers above and below the box indicate the extreme values. Results of Student T-test statistic analysis are noted with a single star (*) for $p<0.05$, and double stars (**) for $p<0.01$. The arrows crossing the y-axis indicate the detection limit of the titration.

Supplementary Fig.6

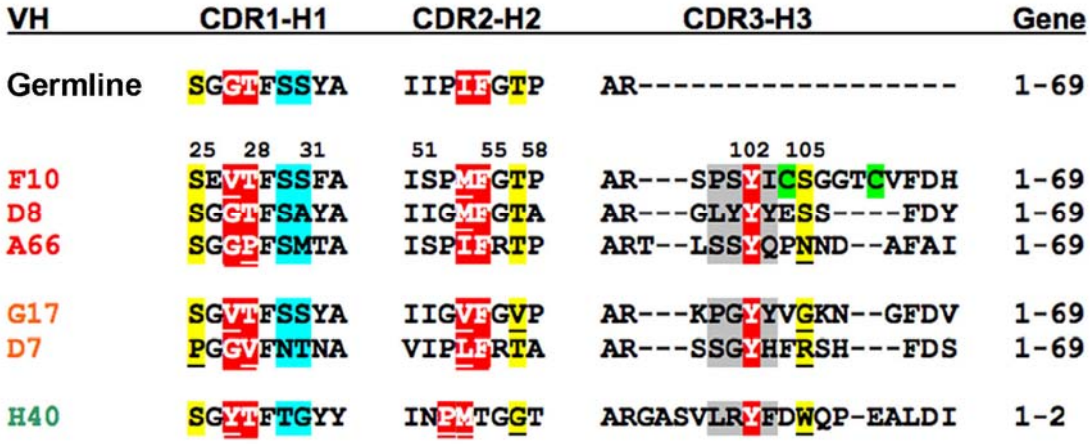

Fig. S6. Sequence conservation within CDR regions of the 6 distinct nAb VH genes. Five genes are derived from the same germline gene, IGHV1-69 ("1-69"), shown on the first line. The CDR3 loop is encoded by other genetic elements. The VL genes (Supplementary Table 1) are much more diverse since they do not contact H5. The 3 VH genes used to make IgG1s are labeled in red. Contact residues are highlighted in different colors based on their estimated contribution to binding: red (very favorable); yellow (favorable); blue (neutral); and gray (unfavorable). Residue differences from the consensus at favorable contacts are underlined. The G=>E mutation at position 26 of F10 induces a non-canonical conformation of H1; the others are predicted to have consensus loop structures. The H2 loop closely follows the consensus "type 2" structure defined by Chothia et al.[1]. The disulfide-bonding pair in the F10 H3 loop is highlighted in green. The H2 loop of the 1-2 gene is predicted to adopt a conformation ("type 3") different from 1-69, in which the highlighted proline and methionine are exposed at its tip. The correspondence of the tyrosine in H3 of H40 is also speculative.

Supplementary Fig. 7

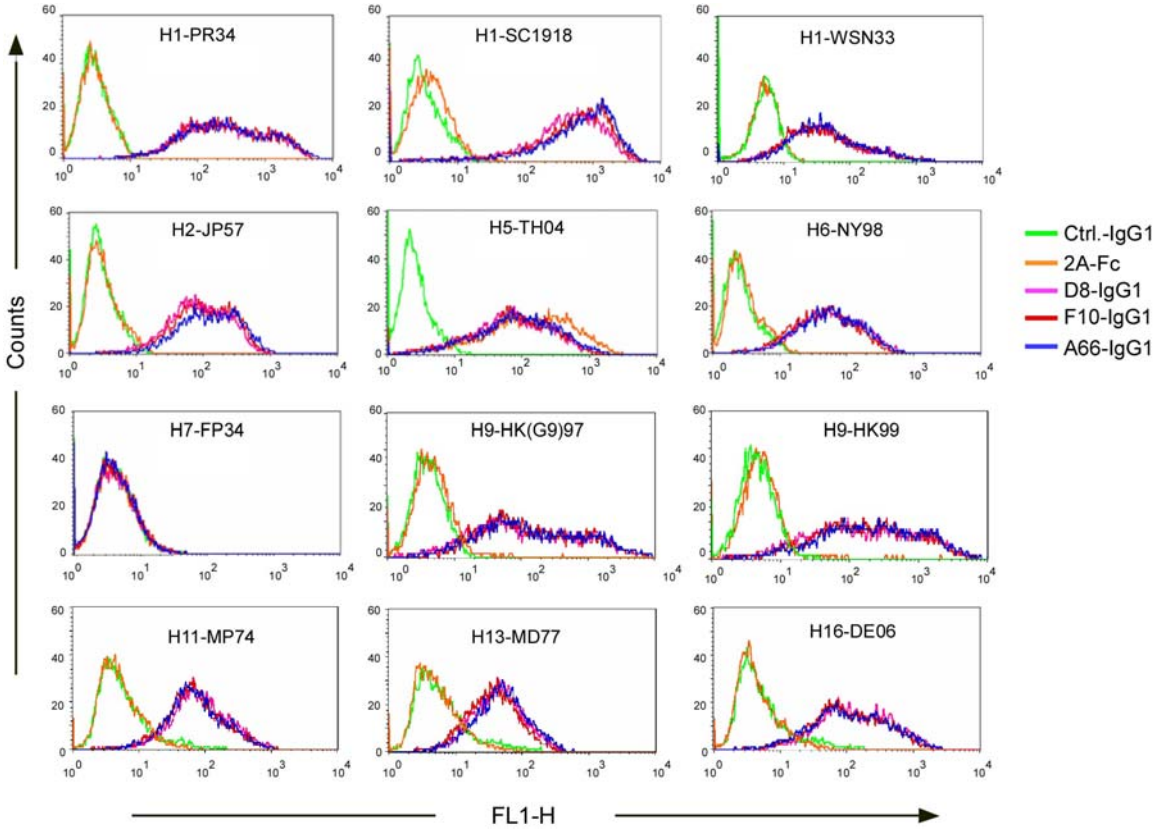

Fig. S7. NAbs bind to a broad range of Group 1 HA subtypes. FACS analysis of anti-H5 nAbs binding to H1, H2, H5, H6 (Cluster H1a), H11, H13 and H16 (Cluster H1b) and H9 (H9 Cluster). 293T cells were transiently transfected with different HA-expressing plasmids, and mAb binding to the cells was analyzed by FACS. H5-specific antibody 2A and 80R are negative control. Lack of binding to a Group 2 HA, H7, is also shown. Complete viral strain designations are: H7-FP34 (A/FPV/Rostock/34 (H7N1)), H13-MD77 (A/gull/MD/704/77 (H13N6)) and H16-DE06 (A/shorebird/DE/172/06 (H16N3)); and see Fig. 6 (main text) for others.

Supplementary Fig. 8

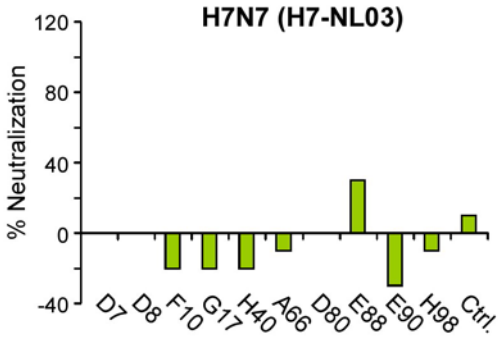

Fig. S8. Anti-H5 nAbs do not neutralize H7N7 influenza virus. 10 H5-selected scFv-Fc Abs were tested for neutralizing activity against H7-NL03 (A/Netherlands/219/2003 (H7N7)) virus in a plaque reduction assay. These results are representative of two independent experiments.

Supplementary Fig. 9

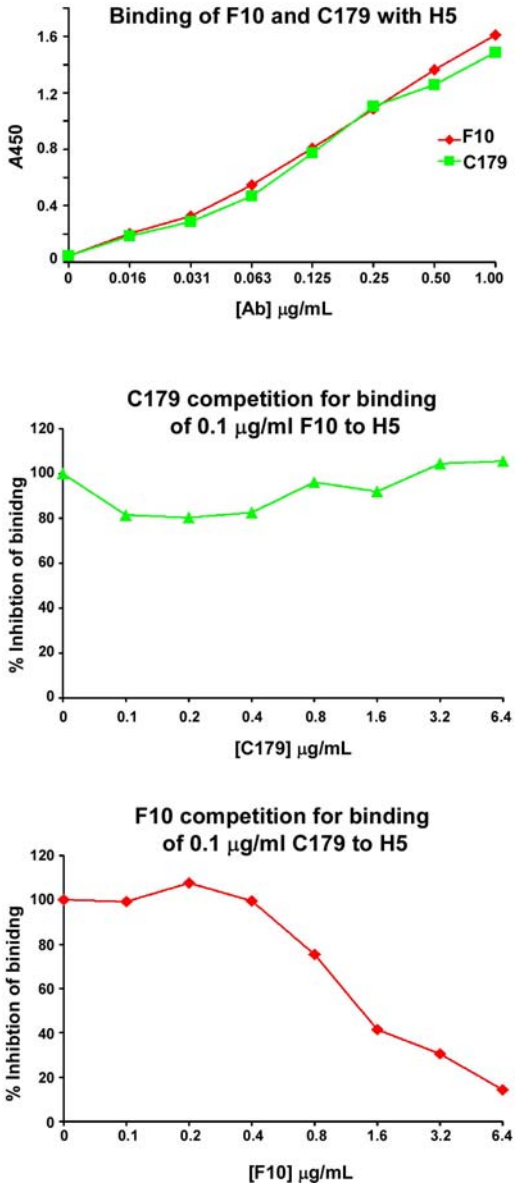

Fig. S9. Binding of F10 or C179 to H5 and cross-competition ELISA for F10 and C179. 0.2 μg of H5 HA proteins were coated onto 96-well ELISA plates for these experiments. Top panel: binding of F10 or C179 to H5 was tested with 2-fold serial dilutions of antibody. Middle and bottom panels: F10 and C179 cross-competition ELISAs. 0.1 μg mL^{-1} C179 or F10 were mixed with different concentrations of F10 or C179.

Supplementary Table 1. Amino acid sequences of variable regions of anti-H5 mAbs

VH	FR1	CDR1	FR2	CDR2	FR3	CDR3	FR4	V GENE
Cons.	KKPGSSVKVSCKAS	GGTFSSYA	ISWVRQAPGQGLEWMGG	IIPMFGTP	NYAQKFQGRVTITADESTSTAYMELSSLRSEDTAVYYC	AR	WGQGTL	
IGHV1-69	....	.GT.SS..	....	...IF.TA	....	..		1-69*01
F10/E90	...........TSS	EVT.SSF.	..............L..	.S.MF.T.	...............Q..R....D.R............	..---SPSYICSGGTCVFDH	......	1-69*01
D8/D80	....	.GT.SA..	FT...............	..GMF.TA	................L...........T.....L...	..---GLYYYESS----FDY	......	1-69*01
A66/E88	....	.GP.SMT.	FT.L.............	.S.IFRT.	K................N..N...T..K..........	..--TLSSYQPNND--AFAI	.....M	1-69*01
G17	....A.......T.	.VT.SS..	....	..GVF.V.	K..............KP...V....N...A........	..---EPGYYVGKN--GFDV	.....M	1-69*06
D7/H98	.............P	.GI.NTN.	F.............V..	V..LFRTA	S...NV...........N......T....A........	..---SSGYHFRSH---FDS	..L...	1-69*01
H40	R...A.........	.YT.TG.Y	.H..............W	.NPMT.GT	.......VW..M.R.T.IN.....VTR.T.D.......	..GASVLRYFDWQP-EALDI	..L..T	1-2
IGHV1-2	....A.........	.YT.TG.Y	MH..............R	.NPNS.GT	...........S.R.T.I........R.....V....	..		

VL	FR1	CDR1	FR2	CDR2	FR3	CDR3	FR4	GENE
Cons.	QPVLTQPPS-ASGSPGQRVTISCTGS		VAWYQQKPGQAPKLLIY		DRPSGIPDRFSGSR--SGTTASLTISGLQPEDEADYYC		FGGGTKLTVL	
D7Vλ	NFM....H.-V.A...KT........	SGNIAANY	.Q....R..S..TTV..	EDD	R....V.......IDR.SNS........KT........	QTYDTNNHAV	.....H....	LV6-57
D8Vλ	.S.......-.......S.......T	SSDVGGYNS	.S....H..K....M..	EVT	K....V.....A.K--..N.....V....A......F.	CSYAGHSAYV	..T...V...	VL2-11
F10Vλ	..G......-V.KGLR.TA.LT...N	SNNVGNQG	A..L..HQ.HP....S.	RNN	......SE...A..--..N......T............	STWDSSLSAVV	....	LV10-54
G17Vλ	SYE......-V.KGLR.TAILT...D	SNNVGHQG	T..L..HQ.HP....S.	RNG	N.....SE...A..--..N......I............	SVWDSSLSAWV	....	LV10-54
H40Vλ	.........-V.VA...TAS.P.G.N	NIGGYS--	.H..........L.V..	DDK	.......E....AN--..S..T....RVEAG..G....	QVWDSGNDRPL	....	VL3-21
A66Vκ	EI....S.ATL.L...E.A.L..RA.	QSVSSY--	L...........R....	DAS	N.AT...A.....G--...DFT....R.E...F.V.F.	QQYGSSPQ---	..Q..R.EIK	KV3-20
D80Vκ	EI....S.GTL.L...E.A.L..RA.	QSLSSKY-	L...........R....	GAS	S.AT.........G--...DFT....R.E...F.V.S.	QQYDGVPRT--	..Q..TVEIK	KV3-20
E88Vλ	L........-...T......I..S..	SSNIGSNT	.N....L..T.......	SNN	Q....V..........--...S...A.I..R........	QSYDSRLSASL	..T..TV...	LV1-44
E90Vκ	DIQM..S..SL.A.V.D....T.RA.	QSISSY--	LN.......K.......	AAS	SLQR.V.S.....G--...DFT....S.....F.V.Y.	QQYDSSPYT--	..Q...VEIK	KV1-39
H98Vλ	SYE......-...KH........S.G	TSNIGRNH	.N....L..T.......	SNE	Q....V.......K--...S...AV....S........	ASWDDNLSGWV	....	LV1-44

Framework regions 1-4 (FR1-4) and complementarity-determining regions 1-3 (CDR1-3) for VH and VL are shown. FR, CDR and gene names are defined using the IMGT database. For VH, the first 11 residues of FR1 (QVQLVQSGAEV) and last 5 residues of FR4 (VTVSS) are invariant and not shown. Dots denote identity with the consensus sequence, hyphens denote gaps. Six different VH and 10 different VL genes were found. 5 out of the 6 VHs belong to one gene family, IGHV1-69 (01 or 06 allele). H40 (colored in blue) uses IGHV1-2 germline gene. The VL genes are much more diverse than the VH genes, consistent with the lack of significant contacts observed between F10 and H5; three out of the 10 VL are κ chain. The 3 VH chains that were used to make IgG1s are colored red. H5 contact residues of F10 observed in the crystal structure are highlighted, along with corresponding residues in other VHs, in cyan (critical residues as defined by FastContact energy calculations) and grey (other contacts < 4.5 Å). Gln74 (important in stabilizing the CDR1 and CDR2 loop conformations) in FR3 is highlighted in green. The H2 loop of H40 is predicted to have a different conformation (see Fig. S6) with different residues at its tip. The residue at position 72 (magenta) largely determines the conformation of the H2 loop (Ala for “type 2” and Arg for “type 3”).

Table S2. Contact residues at the H5-F10 interface

F10	FR-H1	CDR-H1				CDR-H2			CDR-H3				
	Ser25	Val27	Thr28	Ser30	Ser31	Met54	Fhe55	Thr57	Pro100	Ser101	Tyr102	Ile103	Ser105
HA1	Ser291	Ser291 Met292		Gln40		His38	His18 His38						
HA2		Ile56	Trp49 Val52 Asn53		Ile45 Thr49	Trp21 Ile45	Val18 Asp19 Gly20 Trp21	Val18	Gln42	Gln42	Asp19 Lys38 Thr41 Gln42 Ile45	Asp19 Lys38	Lys38

H5-F10 contact residues defined by interatomic distances < 4 Å. The color scheme indicates contributions to the binding energy: very favorable (red); favorable (orange); neutral (blue) and unfavorable (black). For F10, the overall contribution for each residue is shown; for H5, the strength of individual interactions is indicated.

Supplementary Table 3. Sequence comparison of F10 epitope among 16 HA subtypes.

Group	Cluster	Subtype	# Full-length sequence	# Unique sequence	HA1						HA2												
					17	18	38	40	291	292	18	19	20	21	38	41	42	45	49	52	53	56	111
Group 1	H1a	H2	100	95	Y	H	H	(Q,E)/K (18)/77	T	(M)/L (1)/95	(I)/V (20)/75	D	G	W	K	T	Q	(F,V)/I (39)/56	T	(I)/V (1)/94	N	I	H
		H5	1620	1178	(S,T,F)/Y (4)/1174	(Y,M)/H (2)/1176	(Q,Y)/H (4)/1174	(K)/Q (2)/1176	(I,N,T,R)/S (6)/1172	(K,L,I)/M (24)/1154	(I)/V (6)/1172	(N,H,Y,X)/D (5)/1173	G	(R)/W (1)/1177	(Q,R,N)/K (23)/1155	(S)/T (3)/1175	P/Q (1)/1177	(M,L,T)/I (8)/1170	(I)/T (1)/1177	V	N	(F)/ V (1)/1177	H
		H1	1211	701	Y	H	H	(I)V (2)/699	(S)/N 16(685)	(F)/L (1)/700	(I,M)/V (131,6)/546	D	G	W	(K,R,L)/Q (60)/641	T	Q	(V)/I (2)/699	(S,N,X)/T (19)/682	(M,I)/V (2)/699	N	(V)/I (1)/700	H
		H6	278	230	Y	H	H	V	(I)/N (1)/229	(R)/K (4)/226	(V)/I (43)/187	D	G	(R)/W (1)/229	(R)/K (102)/128	T	Q	(V)/I (78)/152	(I)/T (1)/229	(I)/V (3)/227	N	I	H
	H1b	H13	16	16	Y	L	S	(V)/I (6)/10	N	(R)/K (8)/8	I	N	G	W	K	T	Q	I	T	V	N	I	H
		H16	8	6	Y	L	S	(I)/V (2)/6	N	K	I	N	G	W	K	T	Q	I	T	V	N	I	H
		H11	64	64	Y	L	S	(I)/V (1)/64	(T)/S (1)/63	(K)/R (23)/41	(L)/I (1)/63	N	G	W	(R)/K (5)/59	T	Q	(V)/I (3)/61	(I)/T (1)/63	V	N	(I,A)/V (17)/47	H
	H9	H8	10	10	Y	Q	Q	M	S	K	I	D	G	W	Q	T	Q	I	T	(I)/V (1)/9	N	I	H
		H12	19	18	Y	Q	Q	E	S	K	V	A	G	W	R	T	Q	I	Q	L	N	I	H
		H9	252	234	(H)/Y (33)/201	(L)/Q (1)/233	(D)/H (1)/233	(R,E)/K (5)/229	(I)/T (1)/233	(M)/L (1)/233	V	(S)/A (1)/233	G	(G)/W (1)/233	(K,G)/R (14)/220	T	Q	(V,F,M,R)/I (43)/191	(I)/T (1)/233	V	(S,T,D)/N (3)/231	(I)/V (55)/179	(C)/H 1/233
Group 2	H3	H4	105	90	H	H	(A)T (1)/89	(R)Q (1)/89	(A,I,S,N)/T (10)/82	K	I	D	G	(G)/W (1)/91	L	T	Q	I	(N)/T (1)/89	L	N	I	(A)/T (2)/90
		H14	2	2	H	H	S	K	D	K	I	D	G	W	L	T	Q	I	N	L	N	I	T
		H3	2302	1228	H	H	N	(N)/T (1)/1227	(N, Y,E,G)/D (35)/1193	(R,Q,M,N)/K (13)/1215	(M)/(V/I) (149)/(70%/30%)	(N)/D (15)/1213	G	W	(F)/L (1)/1227	T	Q	(V,T,L)/I (5)/1223	(D,S,T,A)/N (22)/1206	(M)/L (1)/1227	(D)/N (1)/1227	(V,T,F)/I (19)/1209	(A)/T (7)/1221
	H7	H15	8	5	H	H	N	T	P	L	I	D	G	W	Y	T	Q	I	T	L	N	I	A
		H7	334	273	H	H	N	T	(S,R,P)/N (131)/142	L	(V)/I (41)232	(N)/D (57)/213	G	W	(H)/Y (1)/272	T	(P)/Q (2)/271	(V)/I (3)/270	T	L	N	I	(T)/A (35)/238
		H10	31	28	H	H	N	T	(E)/K (1)/27	L	V	(N,E)/D (2)/26	(A)/G (1)/27	w	Y	T	Q	I	T	L	N	(V)/I (1)/27	A
# total sequences			6360	4178																			
Rate of non-conservative substitution at positions of major contact residue for both Groups.						2.18% **	2.15% **				0.17% ***	8.70%	0.00%	0.00%	0.05% ****	0.00%	0.00%	4.14%					

This table represents sequences available in public influenza sequence databases (http://www.ncbi.nlm.nih.gov/genomes/FLU/FLU.html) as of April. 17, 2008. Light blue highlights: top '( )/ ', (amino acid variant(s)) / amino acid consensus at the position; bottom '( )/ ', (number of amino acid variants)/ number of consensus amino acids. Non-highlighted amino acids are ~100% conserved or variants are observed ≤ 5 times at those positions for subtypes H4, H6, H9, H10, H11. Histidines H17 (HA1) and H111 (HA2) are buried and may play a role in pH-trigger are highlighted in green. ** H and Q are considered as conserved residues at these positions. *** V and I are both considered as conserved residues. **** Conserved residues include K, R and Q.

Supplementary Notes

Note S1. Epitope conservation and broad neutralization

We analyzed the location of the F10 epitopes in the fusogenic state, using the most complete model of the HA2 triple-helical conformation[2]. The reorganization to form the fusogenic state creates two major features that block access to the epitope observed in the neutral pH structure. First, one face of the αA helix involved in nAb binding becomes buried in the hydrophobic core of the new trimeric helical bundle (comprising residues 37_2-105_2 in H3). A second face of the helix is not obscured by the triple helix; instead it becomes inaccessible by virtue of the packing of a long C-terminal arm ("C-arm") of HA2, the last 23 residues of which form an extended conformation that packs tightly (and anti-parallel) against 2 helices, from residue 76_2 to 38_2.

Thus, considering the F10 epitope residues in αA, Lys 38 is partly-exposed at the base of the new trimeric helix, but makes H-bonds to the C-arm. Thr41 becomes fully buried within the helical trimer, and stabilizes the N-cap of its own helix via its hydroxyl side-chain, while its methyl side-chain combines with its symmetry mates to make the first annulus of the new hydrophobic core. Gln42 remains on the outer surface of trimer, but its side-chain makes H-bonds to two main-chain elements of the C-arm (171 C=O and 173 N), so it is fully obscured. It also stabilizes the conformation of Asp46 (H-bond) which salt-bridges to Arg170 from the C-arm. Ile45 becomes fully buried in the new trimeric core, and together with the preceding Ala44 forms a 6-membered hydrophobic annulus above the Thr41 annulus. Thr49 is exposed on the trimer surface, but makes an H-bond to 169 C=O and a hydrophobic contact with Leu168 (in H3, residues 49 is Asn, which is complemented by a change at position 168, also to Asn, with which it makes a bifurcated H-bond). In the Group 1 viruses, this is the only position with a significant change - Thr49Gln in H12. Simple modeling suggests that there is sufficient space for its side-chains to form H-bonds with 168 and 169 main-chain carbonyls, and also to complement a change at position 47 (Gly47Asn). Val52 becomes completely buried, and forms the next 3-membered annulus of the

hydrophobic core. Asn53 remains exposed on the helical surface, but its side-chain makes H-bonds to both the amide and C=O of residue 168. Finally, Ile56 becomes partly buried, contributing to the next hydrophobic (6-member) annulus with Ile55, and also packing tightly against the C-arm.

```
        38 41  45  49 52  56
         •  •   •   •  •   •
H2   ADKESTQKAVDGITNKVNSIIDK
H5   ADKESTQKAIDGITNKVNSIIDK
H1   ADQKSTQNAIDGITNKVNSVIEK
H6   ADRESTQKAVDGITNKVNSIIDK

H13  ADKESTQKAIDQITTKINNIIDK
H16  ADKTSTQKAINEITTKINNIIEK
H11  ADKESTQKAIDQITSKVNNIVDR

H8   ADQKSTQEAIDKITNKVNNIVDK
H12  ADRDSTQRAIDNMQNKLNNVIDK
H9   ADRDSTQKAIDKITSKVNNIVDK
-------------------------
H3   ADLKSTQAAIDQINGKLNRVIEK
```

We next examined all of the publicly available sequences (Supplementary Table 2). There are 2552 unique sequences for Group 1. When all sequences are considered, exceptions to the consensus are nearly always conservative, and if not very rare (< 0.1%). Of note, H5 is one of the most conserved, with an average of only 2.9 polymorphisms per residue (0.25%) with significant binding energy to F10 (from a data base of 1178 unique sequences). On this basis, and given the variety of CDR sequences in our Ab panel, we believe it reasonable to speculate, pending further data, that our Ab panel will neutralize the majority if not all of the Group 1 subtypes and their polymorphisms. The important point here though is that for those subtypes that are recalcitrant to our current Ab panel, we can simply apply our method to generate a new panel, and assemble a suitable cocktail.

Note S2. Murine mAb C179 neutralization spectrum. As discussed in the main text, C179 neutralized H1N1, H2N2, H5N3 and H5N9 of Group 1 viruses[3,4]. However it did not neutralize an H6 subtype[3]. The commercial vendor of C179 (Takara Bio USA) also provided additional information that it neutralized H9, but not H11 subtypes.

Note S3. Ref. 46 cited in the manuscript. From Table 1 of this reference (Kashyap, A. K. et al. Proc Natl Acad Sci U S A 2008, 105: 5986-91) we can deduce, based on the IMGT database (http://imgt.cines.fr/), that the VH germline gene used by these nAbs is VH1-69, previously designated as VH1e as reported.

Note S4. A recent report (Wrammert J. et al, Nature, 2008 453:667) sheds new light on this question. Data in this paper indicates that the humoral immune response against influenza virus is characterized by a highly restricted B-cell receptor repertoire in nature, and that more than half of the HA-specific human antibodies identified from antibody secreting cells (ASC) of influenza-vaccinated humans are raised against the globular head of HA (HA1) (This latter conclusion was not explicitly stated by the authors, but can be deduced from the data). Their data show that half of the HA-specific Abs are HI (hemagglutination inhibition) positive. Since some portion of HI-negative Abs are also HA1 specific, we can conclude that more than half of the HA-specific Abs are against HA1. The HA1 globular head is well-exposed and could be readily recognized by B cell receptors, and immune responses to this region are dominant in the vaccination procedure or by natural infection. Yet most if not all antibodies induced by this region lack cross-neutralizing-activity, owing to the great variability of HA1. Meanwhile, for conserved epitopes like the F10 epitope identified in our study, there may be a paucity of opportunities for B-cells to engage the epitope, and thus the host fails to mount a timely and productive neutralizing antibody response; or the Ab response against the F10-like epitope may be precluded due to other unknown mechanism(s).

Note S5. nAbs D8, F10 and A66 lack of autoreactivity. The three nAbs were tested for binding to self-antigens using standard clinical assays. The results show that the three nAbs do not bind to the following self-antigens: dsDNA, histone, Sm/RNP, SS-A, SS-B, Scl-70, centromere, PCNA, Jo-1, mitochondria, ribosomal-P protein, 60KD SS-A/Ro, Hep-2 cell extracts as well as cardiolipin. The highest antibody concentration tested in these assays is 100-200 μg mL^{-1}. Assays were performed using ELISA for detecting anti-nuclear antibodies (ANA) (QUANTA lite™ ANA ELISA kit, INOVA Diagnostics, Inc), ELISA for detecting anti-cardiolipin antibody (RELISA cardiolipin IgG kit, ImmunoConcepts Inc.) and HEP-2000 cell immunoflurecence (ImmunoConcepts Inc.).

Note S6. Small molecule inhibitors. Several small molecule inhibitors have been shown to neutralize influenza virus by inhibiting membrane fusion, although they lack broad cross-subtype neutralization, and are prone to immune escape. Russell et al.[5] have recently demonstrated crystallographically that a small molecule inhibitor of membrane fusion (specific to the Group 2, H3 cluster), TBHQ, binds in a cavity behind the “pocket” that is present in Group 2 but not Group 1 viruses[5]. In addition, an inhibitor of Group 1 viruses (H1 and H2 subtypes), BMY-27709, also acts by blocking membrane fusion, and its binding site has been tentatively mapped to $Phe110_2$, based on the ability of a Phe-Ser mutant to escape inhibition[6]. It may act by interfering with the $His111_2$-mediated pH trigger that is present in Group 1 but not Group 2 viruses. Most such inhibitors neutralize viruses with an IC_{50} in the μM range. *In vivo* efficacy data for these inhibitors are also currently lacking.

Supplementary Materials and Methods

Viruses, cells, HA and NA expressing plasmids. Wild type influenza A/Vietnam/1203/2004 (H5N1; H5-VN04), A/HongKong/483/1997 (H5N1; H5-HK97), A/Netherlands/219/2003 (H7N7; H7-NL03), , A/WSN/N/1933 (H1N1, H1-WSN33) and A/Ohio/4/1983 (H1N1; H1-OH83) viruses as well as a cold-adapted vaccine strain of A/Ann Arbor/6/1960 (H2N2; H2-AA60) , A/Sydney/5/97 (H3N2; H3-SY97), A/quail/Hong Kong/1721-30/99 (H6N1, H6-HK99), A/Chicken/New York/14677-13/1998 (H6N2; H6-NY98), H7-FP34 (A/FPV/Rostock/34 (H7N1)), A/turkey/Onatario/6118/68(H8N4; H8-ON68), A/chicken/HongKong/G9/97 (H9N2; H9-HK(G9)97), A/HongKong/1073/99 (H9N2, H9-HK99) were obtained from the WHO Global Influenza Surveillance Network and provided by Alexander Klimov (CDC, Atlanta, USA). A/Puerto Rico/8/1943 (H1N1; H1-PR34), Madin-Darby canine kidney (MDCK), Hela and 293T cells were obtained from the American Type Culture Collection and propagated in Dulbecco's Modification of Eagle's Medium with 10% fetal bovine serum. Viral infectivity was determined by plaque assay on MDCK cells. Live wild-type H5N1 viruses were handled in biosafety level 3 containment, including enhancements required by the U.S. Department of Agriculture and the Select Agents program http://www.cdc.gov/od/ohs/biosfty/bmbl5/bmbl5toc.htm. The full length HA gene (H5-TH04) of A/Thailand/2(SP-33)/2004 (H5N1) and neuramidase gene (N1) of H5-VN04 (Genbank accession AAW80723) were codon-optimized for eukaryotic cell expression and cloned into pcDNA3.1 vector to obtain the pcDNA3.1-H5-TH04 and pcDNA3.1-N1 expressing plasmids, separately. Full length HA subtypes including H1-WSN33, H2-AA60, , H6-NY98, H9-HK(G9)97, H9-HK99, H11(A/duck/Memphis/546/1974 (H11N9)), H13 (A/gull/Maryland/704/1977 (H13N6)) and H16 (A/shorebird/Delaware/172/2006 (H16N3)) were directly cloned from viral RNA and further subcloned into a pcDNA3.1 expression vector. See Acknowledgements for details on other subtype HAs.

HA1 is an N-terminal fragment of HA of H5N1 A/Thailand/2(SP-33)/2004 (H5-TH04), residues 11 to 325 (H3 numbering). The gene was codon-optimized for eukaryotic cell expression and expressed as fusion protein with a C-terminal 9 amino-acids tag (C9-tag: GTETSQVAPA). The fusion protein HA1-C9 was expressed in 293T cells transiently and the secreted proteins in supernatant were harvested 48 hours after transfection and purified from the supernatant by affinity chromatography using Protein A Sepharose that was coupled covalently with anti-C9 antibody 1D4 (National Cell Culture Center).

Expression and preparation of phage-scFvs, soluble scFv-Fcs and full-length human IgG1. Phage-scFvs of individual clones were produced as described previously[7]. scFv-Fcs and whole human IgG1 were produced as described previously[7-9]. In brief, selected scFvs were converted to scFv-Fcs by subcloning the scFv into an Fc expression vector pcDNA 3.1-Hinge, which

contains the hinge, CH2, and CH3 domains of human IgG1 but lacks CH1. For whole human IgG1s, the VH and VL gene fragments of scFv were separately subcloned into human IgG1 κ light chain or λ light chain expression vector TCAE5 or TCAE6[9]. scFv-Fcs or IgG1s were expressed in 293T or 293F cells (Invitrogen) by transient transfection and purified by protein A sepharose affinity chromatography.

ELISA. 0.2 μg of pure H5 HA proteins were coated onto 96-well Maxisorb ELISA plates (Nunc, NY) at 2 μg mL^{-1} in PBS at 4ºC overnight. The plates were washed 3 times with PBS to remove uncoated proteins. For regular ELISA, 1 μg mL^{-1} of anti-H5 scFv-Fcs followed by HRP-anti-human IgG1 were used to detect the binding of anti-H5 scFv-Fcs to H5 HA proteins. For competition ELISA, 50 μL(10^{12} pfu) of anti-H5 phage-scFvs were mixed with 5 μg mL^{-1} of anti-H5 scFv-Fcs and applied to H5-VN04 HA-coated ELISA plates. The competition of scFv-Fcs for the binding of phage-scFvs to HA0 was determined by measuring the remaining binding of phage-scFvs using HRP-anti-M13. The optical density at 450 nm was measured after incubation of the peroxidase tetramethylbenzidine (TMB) substrate system (KPL, Gaithersburg MD).

Haemagglutination inhibition (HI) assay. The HI assay was performed as previously described[10]. Briefly, H5N1/PR8[11], H5-VN04 and H1-PR34 viruses were mixed with log_2 antibody dilutions in PBS, and incubated at 20-22ºC for 30 min. A 0.5% suspension of turkey erythrocytes was added to each well, and the mixture incubated for 30 min at RT before visual scoring for haemagglutination activity.

Binding of anti-HA5 antibodies with H5-TH04 mutants. All mutants of pcDNA3.1-H5-TH04 were constructed by the QuikChange method (Stratagene, La Jolla, CA). Various full-length wild type HA and HA mutants expressing plasmids of H1, H5 or H7 were transfected transiently into 293T cells. 24 h after transfection, cells were harvested for immunostaining. Anti-H5 or control mAb 80R[7] at 10 μg mL^{-1} or ferret anti-H5N1 serum at 1:300 dilution were incubated with transfected 293T cells at 4ºC for 1 h. Cells were then washed three times with PBS containing 0.5% BSA and 0.1% NaN_3. FITC-labeled goat anti-human IgG (Pierce Biotech., Rockford, IL) or FITC-labeled goat anti-ferret IgG (Bethyl, Montgomery, TX) were then added to cells and incubated for 30 mins at 4ºC. Cells were washed as above, and binding of antibodies to cells was analyzed using a Becton Dickinson FACScalibur with CellQuest software.

Neutralization assay with HA-pseudotyped viruses. We produced the single-round HIV luciferase reporter viruses pseudotyped with viral envelopes of H5-TH04, H1-SC1918, H1-PR34, H2-JP57, H6-NY98 or H11-MP74 (See Supplementary Materials) by co-transfection of 293T cells with 4 plasmids: HA-expressing plasmid, HIV packaging vector pCMVΔR 8.2 encoding HIV-1 Gag-Pol; transfer vector pHIV-Luc encoding the firefly luciferase reporter gene under

control of the HIV-1 LTR; and N1-expressing plasmid pcDNA3.1-N1. The ratio of H5- to N1-expressing plasmids was 4:1. After 8-12h transfection, the medium was changed to serum-containing medium (for H5) or serum-free DMEM medium supplemented with 0.2% (w/v) BSA (for H1, H2, H6 and H11). Viral supernatants were harvested at 36h post-transfection. Prior to neutralization tests, supernatants containing pseudotyped viruses (except H5N1) were incubated with 16 μg ml^{-1} TPCK-treated trypsin for 1h at 25°C, and then neutralized with trypsin-neutralizing solution (TNS, Cambrex) at a ratio of 1:1 (v/v). The neutralization assay was performed as previously described[12]. Viral entry level was evaluated by measuring luciferase activity in target cells.

Surface Plasmon Resonance (SPR) analysis. Kinetic analyses of H5 HA mAbs binding to recombinant H5-VN04 HA0 trimer were performed on a Biacore T100 (Biacore, Sweden) at 25ºC. Anti-human IgG Fc antibody (Biacore) was covalently attached to individual flow cell surfaces of a CM4 sensor chip by amine-coupling using the amine coupling kit (Biacore). HA mAbs were captured onto anti-human IgG Fc surfaces (flow rate of 10 μl min^{-1} in HBS buffer (Biacore)) to ensure that mAb-H5 binding occurred as a homogenous 1:1 Langmuir interaction. H5 HA was injected over each flow cell at a flow rate of 30 μl min^{-1} in HBS buffer, and at concentrations ranging from to 0.31 to 20 nM. A buffer injection served as a negative control. All experiments contained an additional anti-human IgG Fc antibody control surface that accounted for changes in the buffer refractive index and to test for potential nonspecific interactions between H5 HA and anti-human IgG Fc. Upon completion of each association and dissociation cycle, surfaces were regenerated with 3 M $MgCl_2$ solution. The association rates (*ka*), dissociation rates (*kd*), and affinity constants (K_D) were calculated using Biacore T100 evaluation software. The quality of each fit was based on the agreement between experimental data and the calculated fits, where the Chi^2 values were below 1.0. Surface densities of mAbs against H5 HA were optimized to minimize mass transfer and avoid any contribution of avidity effects. All *ka, kd,* K_D values reported here represent the mean and standard error of three experiments.

In vivo inhibition by nAbs of virus replication in lung, brain and spleen. Three human nAbs (D8-IgG1, F10-IgG1 and A66-IgG1) or control nAb 80R-IgG1 were administered at 15 mg kg^{-1} into groups of 10 mice by intraperitoneal (i.p.) injection in a volume of 0.5 mL 24h, 48h and 72h after inoculation with $10xMLD_{50}$ of H5-VN04 or H5-HK97 by the intranasal (i.n.) route. To determine viral titers in different organs of H5-VN04-infected mice, 5 animals in each group were euthanized at 4 days post-inoculation, and the lungs, brains, and spleens were aseptically removed and homogenized. Viral infectivity titers in homogenized tissue suspensions were determined by plaque assay on monolayers of MDCK cells. The viral titer is expressed as plaque-forming units per gram (pfu g^{-1}) of tissue. The remaining 5 mice were weighed and observed for 2 weeks after inoculation. Body weight was recorded daily for two weeks.

Expression and purification of F10 scFv and H5 for crystalization.

The gene encoding F10 scFv (VH-linker-VL) was cloned into a pSynI vector containing an N-terminal periplasmic secretion signal, pelB, and a C-terminal His_6 tag. F10 scFv was expressed in XL10 cells in 2YT media containing 0.1% glucose (w/v) at 25°C for 15h with 0.5 mM IPTG. Protein was purified first by Hisbind Ni-NTA (Novagen) according to the manufacturer's instructions, and then by Superdex 200 (Amersham Biosciences) in 50 mM Tris-HCl, 0.5 M NaCl, pH 8.

The ectodomain of H5-VN04 HA gene was expressed in insect cells as a fusion protein by adapting the protocol described previously[13]. This construct contains a C-terminal trimerizing 'foldon' sequence from the bacteriophage T4 fibritin to stabilize the trimeric structure, followed by a thrombin site and a His_6 tag. The cDNA of the fusion protein was cloned into the baculovirus transfer vector, pAcGP67A (BD Biosciences, Bedford, MA), to allow for efficient secretion of recombinant protein. To obtain fully cleaved HA (as HA1-HA2 trimers), sf9 cells were co-infected with baculovirus stocks of HA0 and furin at an empirically derived ratio. The furin cDNA was a gift from Dr. Robert Fuller (University of Michigan). Three days after infection, the cells were spun down and the supernatant was incubated with Ni-NTA beads (Qiagen Inc., Valencia, CA). The beads were washed with TBS buffer (10 mM Tris.HCl, 80 mM NaCl, pH 8.0) with 10 mM imidazole, and eluted with TBS with 250 mM Imidazole. The eluted H5 protein was dialyzed against TBS buffer and further purified by ion-exchange using Mono Q HR10/10 column (GE Healthcare, Piscataway, NJ). The purified H5 was digested by thrombin overnight and further purified by Superdex 200 column in TBS buffer.

Comparison of two trimers in asymmetric unit. The RMS differences between our refined H5 trimers in the F10 complex and the H5 starting model (2IBX) are 1.0 and 0.63 Å for all Cαs. The value for the second trimer is close to that expected on the basis of random error alone; the larger value for the first arises from a twist of the stem region with respect to the head by a few degrees about a vertical axis. When the two copies of the complex are superposed, the head regions overlay closely, but the stems diverge as a function of distance both from the head and from the 3-fold axis, such that the outer parts of the stem at the Ab interface shift by ~3 Å. However, this does not affect the antibody-antigen contacts, and 3-fold symmetry is maintained. These differences explain why 6-fold or 2-fold non-crystallographic symmetry (ncs) refinement was unsuccessful, although, in retrospect, we could have used 2x3-fold ncs with distinct masks for the two trimers. However, refinement without ncs converged successfully, utilizing the high resolution starting models fitted locally to the refined models after each round of automatic refinement as guides during model-building.

References

1. Chothia, C. et al. Structural repertoire of the human VH segments. *J Mol Biol* **227**, 799-817 (1992).
2. Chen, J., Skehel, J.J. & Wiley, D.C. N- and C-terminal residues combine in the fusion-pH influenza hemagglutinin HA(2) subunit to form an N cap that terminates the triple-stranded coiled coil. *Proc Natl Acad Sci U S A* **96**, 8967-72 (1999).
3. Smirnov, Y.A. et al. An epitope shared by the hemagglutinins of H1, H2, H5, and H6 subtypes of influenza A virus. *Acta Virol* **43**, 237-44 (1999).
4. Okuno, Y., Isegawa, Y., Sasao, F. & Ueda, S. A common neutralizing epitope conserved between the hemagglutinins of influenza A virus H1 and H2 strains. *J Virol* **67**, 2552-8 (1993).
5. Russell, R.J. et al. Structure of influenza hemagglutinin in complex with an inhibitor of membrane fusion. *Proc Natl Acad Sci U S A* (2008).
6. Luo, G. et al. Molecular mechanism underlying the action of a novel fusion inhibitor of influenza A virus. *J Virol* **71**, 4062-70 (1997).
7. Sui, J. et al. Potent neutralization of severe acute respiratory syndrome (SARS) coronavirus by a human mAb to S1 protein that blocks receptor association. *Proc Natl Acad Sci U S A* **101**, 2536-41 (2004).
8. Gould, L.H. et al. Protective and therapeutic capacity of human single-chain Fv-Fc fusion proteins against West Nile virus. *J Virol* **79**, 14606-13 (2005).
9. Reff, M.E. et al. Depletion of B cells in vivo by a chimeric mouse human monoclonal antibody to CD20. *Blood* **83**, 435-45 (1994).
10. Donald, H.B. & Isaacs, A. Counts of influenza virus particles. *J Gen Microbiol* **10**, 457-64 (1954).
11. Subbarao, K. et al. Evaluation of a genetically modified reassortant H5N1 influenza A virus vaccine candidate generated by plasmid-based reverse genetics. *Virology* **305**, 192-200 (2003).
12. Sui, J. et al. Evaluation of human monoclonal antibody 80R for immunoprophylaxis of severe acute respiratory syndrome by an animal study, epitope mapping, and analysis of spike variants. *J Virol* **79**, 5900-6 (2005).
13. Stevens, J. et al. Structure and receptor specificity of the hemagglutinin from an H5N1 influenza virus. *Science* **312**, 404-10 (2006).